PARAMETRIC ANALYSIS OF CANDU NEUTRON TRANSIENTS

PARAMETRIC ANALYSIS OF CANDU NEUTRON TRANSIENTS

by

THOMAS ROBERT MCCORMICK, B.Sc.

PART B

A Report
Submitted to the School of Graduate Studies
in Partial Fulfillment of the Requirements for
the Degree
Master of Engineering

McMaster University

1981

One of two project reports: The other part is designated as Part A

MASTER OF ENGINEERING (1981) McMASTER UNIVERSITY
Engineering Physics Hamilton, Ontario

TITLE: Parametric Analysis of CANDU Neutron Transients

AUTHOR: T.R. McCormick, B.Sc. (Queen's, Kingston)

SUPERVISOR: A.R. Dastur (AECL)

NUMBER OF PAGES: vii, 52

ABSTRACT

A fundamental and important part of nuclear reactor development and analysis today is the study of neutronics following a breach in the primary heat transport circuit. In the past, much of this analysis has concentrated on the calculation of the thermalhydraulic changes which occur following a loss of coolant accident and the effects these subsequently have on neutron kinetics. The purpose of this present study is to examine the influence of neutronic parameters on the size and shape of power pulses which result from loss of coolant accidents. The parameters studied are shutdown system delay times, shutoff rod drop curves, and fuel burnup distribution.

ACKNOWLEDGEMENTS

With any industrial project, invariably many people play a part, and the author would like to take this opportunity to thank all of the people who assisted in this report.

The author would like to express his gratitude to his supervisor, Adi Dastur (AECL), for his invaluable guidance, direction and encouragement during the course of this work. It has been a privilege to work, argue and learn with him.

Thanks are due to Dr. A.C. Whittier (AECL) for allowing me the opportunity to do this work and for his encouragement throughout its progress.

The author is greatly indebted to Dr. D.H. Chung (AECL) for his assistance, suggestions and criticisms on aspects of the studies, and to F. Piva (AECL) for his setting up and execution of the point kinetics computations in Chapters 6.1 and 6.2.

A kudo is gratefully given to Mrs. B. McKee for her patience and humour while typing this report.

Lastly, this work is dedicated to my sister, brother, brother-in-law and friends, all of whom taught me how to cooperate with people.

TABLE OF CONTENTS

LIST OF FIGURES

LIST OF TABLES

CHAPTER 1

INTRODUCTION

Prior to a system perturbation, the reactor core is assumed to be in a steady-state situation at some constant power level. An irregularity occurs in the primary heat transport system, and various regions of the reactor core begin to experience a loss-of-coolant. The initial affect of this voiding of the coolant is a general increase in the system reactivity of the reactor core (See Chapter 3). The power of the core starts to rise due to the increased neutron multiplication brought on by this extra reactivity. Radiation detectors throughout the core monitor these changes and trigger the reactor shutdown systems when either power levels or power level rate of rise exceed preset trip levels. The power continues to rise as the shutdown system is activated, and the increase continues until the negative reactivity introduced by the shutdown devices causes the prompt neutron removal rate to exceed the delayed neutron source. At this point, the reactor power starts to decrease. Increasing shutdown activity accelerates the rate of power level decrease until the maximum shutdown reactivity is reached. After that, the power level continues to decay as neutron and non-neutron power sources (long-life γ sources, photoneutrons, spontaneous fission, etc.) continue in the reactor core. From the brief description given above, the various neutronic parameters of this study can be outlined. These are:

(i) Delay times before shutdown activity is initialed (Regions A and B in Figure 1.1). These determine both the level and rate of increase the power pulses reach before counteracting effects (i.e., the shutdown systems) come into play. There are 3 main sources of delay:

a) Signal-generation delay. The current generated by the in-core flux detectors is caused by detector electrons liberated by reactor γ-rays or neutron capture. Neutron capture in the detector materials results in the creation of radionuclides which then emit electrons by β-decay, or γ-decay causing Compton and photo-electric processes. Both of these processes introduce a time delay factor into the signal generation process of the in-core detector.

b) Electronic processing delay. All of the signals from the detectors must be processed in some form, e.g., by amplification, or, if the rate of power increase is being measured, by electronic differentiation. All of these introduce an electronic delay factor into the signal circuit due to capacitance charging, semiconductor dwell times, etc.

c) Mechanical delays. All shutdown systems, being primarily mechanical devices, have an inherent delay before their responsive motion begins. For shutoff rods, this is the deactivation of the electromechanical clutch holding them in place; for poison-injection systems, it is the opening of the high-speed injection valves.

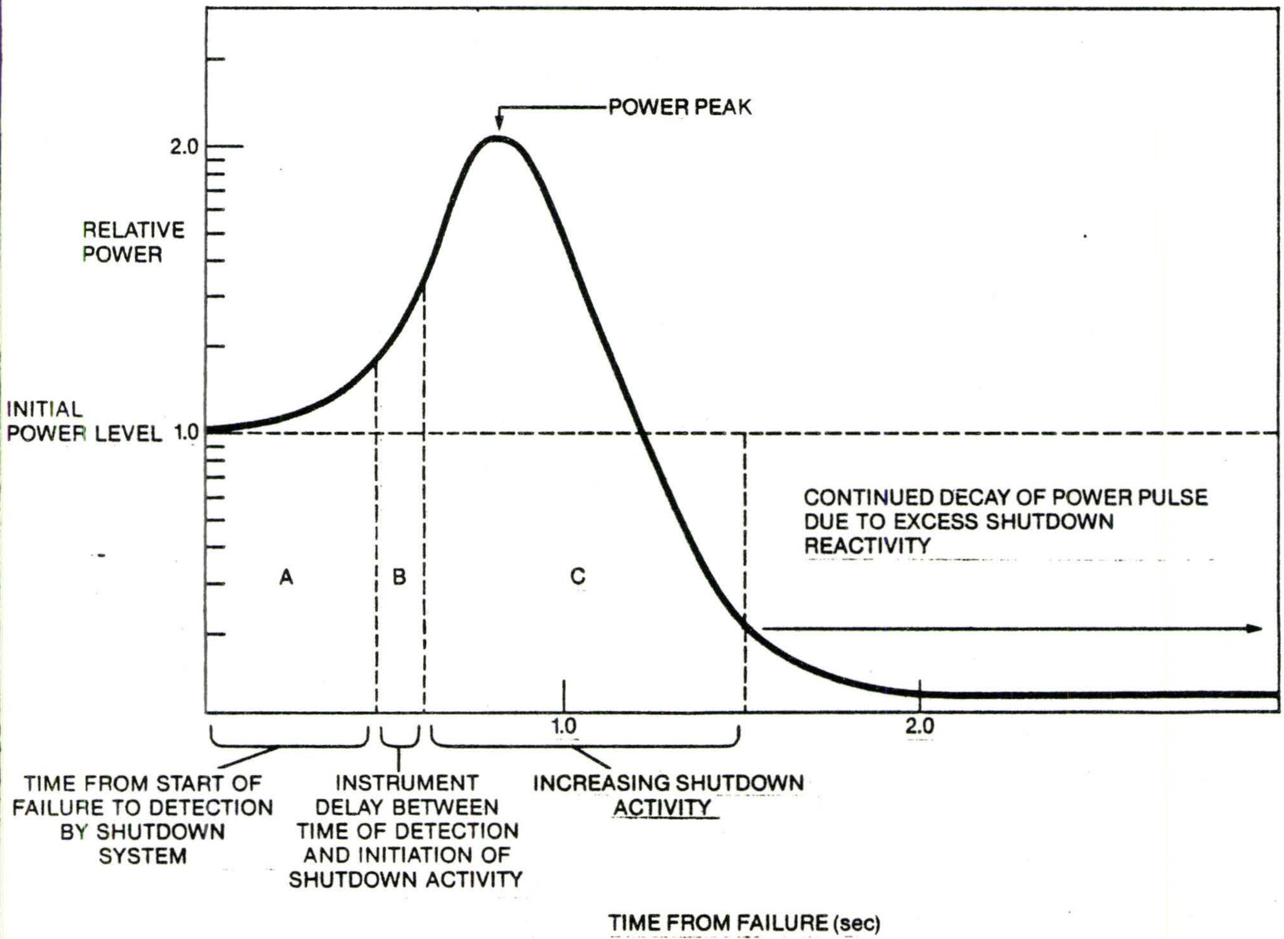

FIGURE 1.1 **TYPICAL POWER PULSE FOLLOWING LOCA**

(ii) Shutdown reactivity transients (Region C). Of importance here are both the magnitude of the reactivity transient and its rate of change. This was studied extensively with respect to the shutoff rod shutdown system since, by the nature of their falling through the reactor core, the spatial and magnitude variation of their reactivity can be greatly altered by various parameter changes.

(iii) Fuel burnup distribution. The effect of the void distribution with respect to the fuel burnup values of the voiding channels was studied as to how the fuel burnup distribution affects the power pulse shape and size following a LOCA.

In all cases, the postulated accident is a reactor loss-of-coolant accident. Although an occurrence of extremely low probabiltiy, this is a severe test of the ability of the shutdown systems to respond to and shutdown the reactor before any fuel damage is done. As a result of this, the shutdown systems of CANDU reactors are built with very fast response times ($\sim$ 0.3 - 0.5 seconds) to safely handle this "worst-case" scenario.

CHAPTER 2

CANDU REACTOR SYSTEM

2.1 Reactor Core

A standard CANDU-PHW reactor consists of a cylindrical stainless steel calandria structure containing heavy water moderator, reactivity control mechanisms and fuel channels (Figure 2.1). The fuel channels contain fuel bundles and high temperature, pressurized heavy water coolant. The main heat transport system circulates pressurized heavy water through the fuel channels to remove heat produced by fission. The heat is transferred in the steam generators to ordinary water to form steam to drive the turbine generators. Two circulation passes are provided so that flow is in one direction through one half of the fuel channels and in the opposite direction through the other half. The heavy water moderator is also provided with a cooling system to dissipate heat transferred to it from the fuel channels.

The reactor is fuelled with natural uranium in the form of uranium dioxide pellets (UO_2). These pellets are assembled into fuel bundles, with each fuel channel accommodating twelve bundles.

2.2 Heat Transport System

The main heat transport system removes heat from the reactor core by the circulation of pressurized heavy water through the reactor fuel channels (Figure 2.3) and two independent figure-of-eight circuits are used. They are interconnected only via a pressurizer and a purification system (Not shown in Figure 2.3). Thus, if a break suddenly occurs

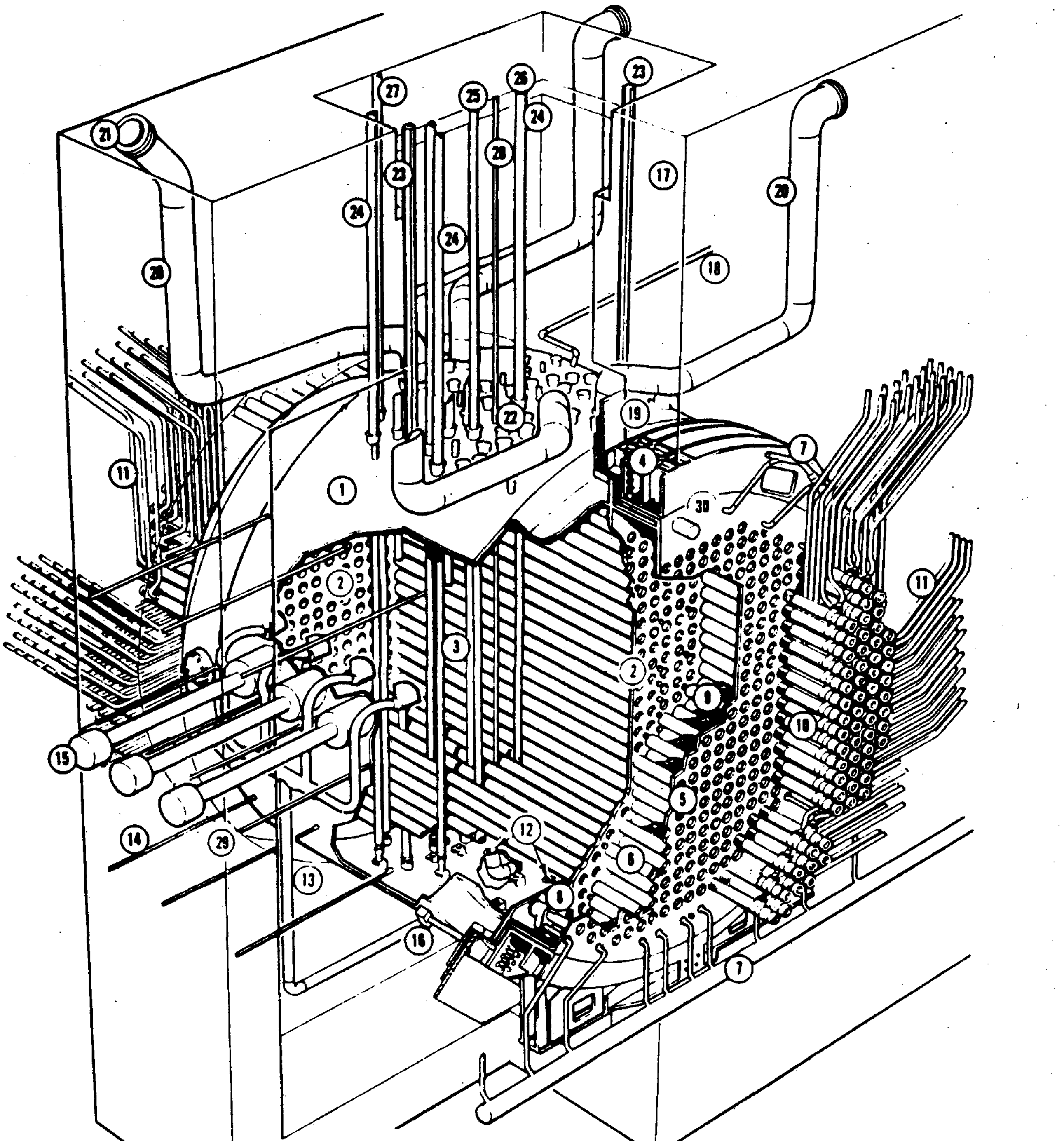

1	CALANDRIA	16	EARTHQUAKE RESTRAINT
2	CALANDRIA – SIDE TUBESHEET	17	CALANDRIA VAULT WALL
3	CALANDRIA TUBES	18	MODERATOR EXPANSION TO HEAD TANK
4	EMBEDMENT RING	19	CURTAIN SHIELDING SLABS
5	FUELLING MACHINE – SIDE TUBESHEET	20	PRESSURE RELIEF PIPES
6	END SHIELD LATTICE TUBES	21	RUPTURE DISC
7	END SHIELD COOLING PIPES	22	REACTIVITY CONTROL UNIT NOZZLES
8	INLET-OUTLET STRAINER	23	VIEWING PORT
9	STEEL BALL SHIELDING	24	SHUTOFF UNIT
10	END FITTINGS	25	ADJUSTER UNIT
11	FEEDER PIPES	26	CONTROL ABSORBER UNIT
12	MODERATOR OUTLET	27	ZONE CONTROL UNIT
13	MODERATOR INLET	28	VERTICAL FLUX DETECTOR UNIT
14	HORIZONTAL FLUX DETECTOR UNIT	29	LIQUID INJECTION SHUTDOWN NOZZLE
15	ION CHAMBER	30	BALL FILLING PIPE

FIGURE 2.1 REACTOR ASSEMBLY

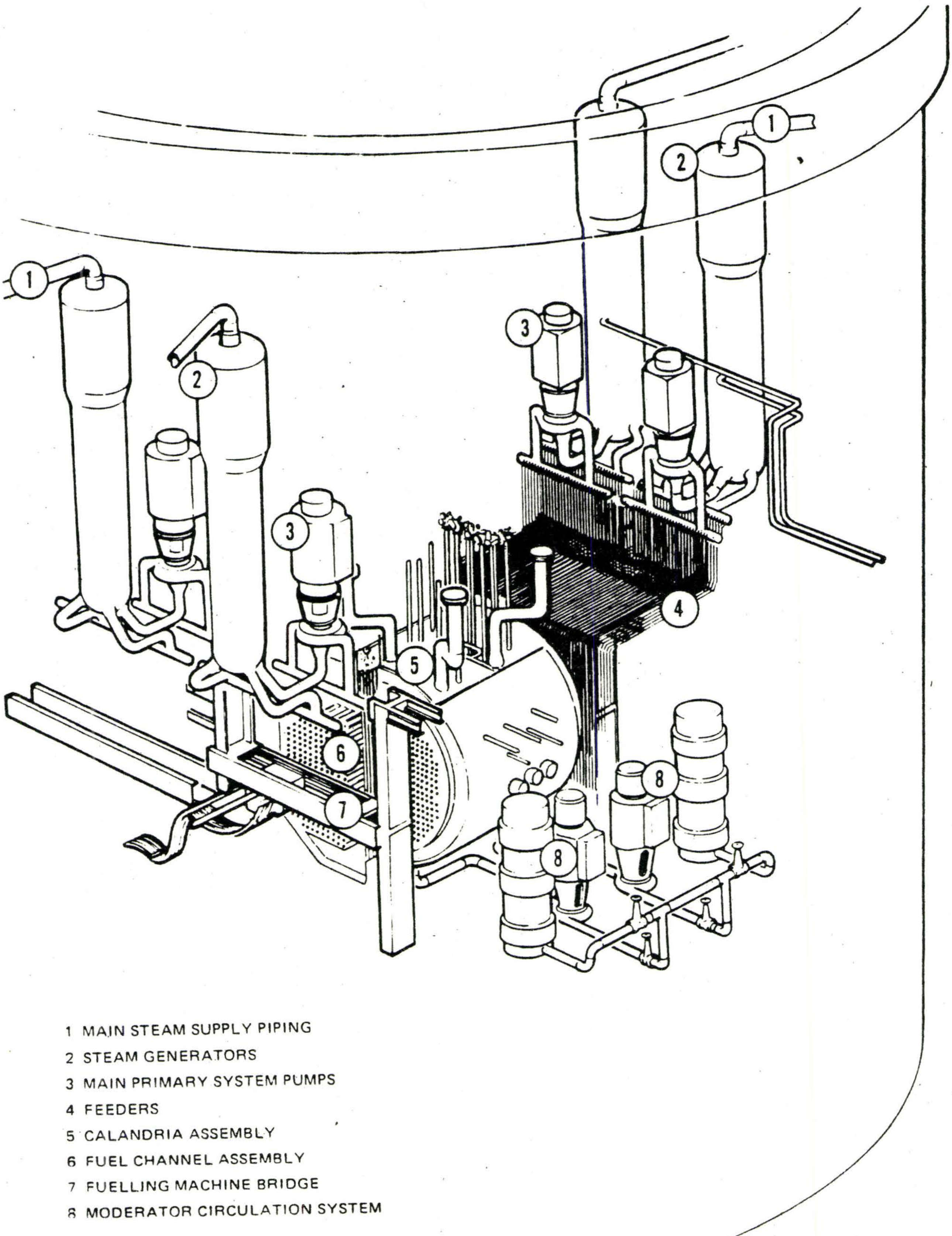

1 MAIN STEAM SUPPLY PIPING
2 STEAM GENERATORS
3 MAIN PRIMARY SYSTEM PUMPS
4 FEEDERS
5 CALANDRIA ASSEMBLY
6 FUEL CHANNEL ASSEMBLY
7 FUELLING MACHINE BRIDGE
8 MODERATOR CIRCULATION SYSTEM

FIGURE 2.2 NUCLEAR CORE SYSTEM AND STEAM GENERATING PLANT

in one circuit, the loss-of-coolant effect is confined to half of the core. Also, an advantage of the figure-of-eight arrangement is that, in the event of a heat transport pump failure, coolant flow in the circuit can be maintained at approximately 70% of the normal value due to the presence of the other pump.

There are two circulation loops, or passes, with adjacent fuel channels being in separate loops. Heat transport pumps in each circulation loop maintain a steady fluid flow through the system at all times. Each heat transport pump is provided with a flywheel so that the pump unit maintains pump operation after loss of motor power. This emergency fluid flow approximately matches the power rundown following a reactor trip. Natural convection following pump rundown is sufficient for shutdown heat removal.

In the study of CANDU accident analysis, the various loss-of-coolant accidents are modelled by considering various sizes of breaks in the fluid flow at crucial parts of the coolant circuit. Referring to Figure 2.3, these are:

(1) Pump suction break. In this case, one of the primary heat transport pumps is assumed to rupture, resulting in a loss of coolant out of the break. The break is expressed as a percentage of twice the cross-sectional area and is modelled as a hole based on this premise. Thus, a 90% Pump Suction break is modelled by the thermalhydraulic codes as a hole with 1.8 times the cross-sectional area of the pipe at the pump.

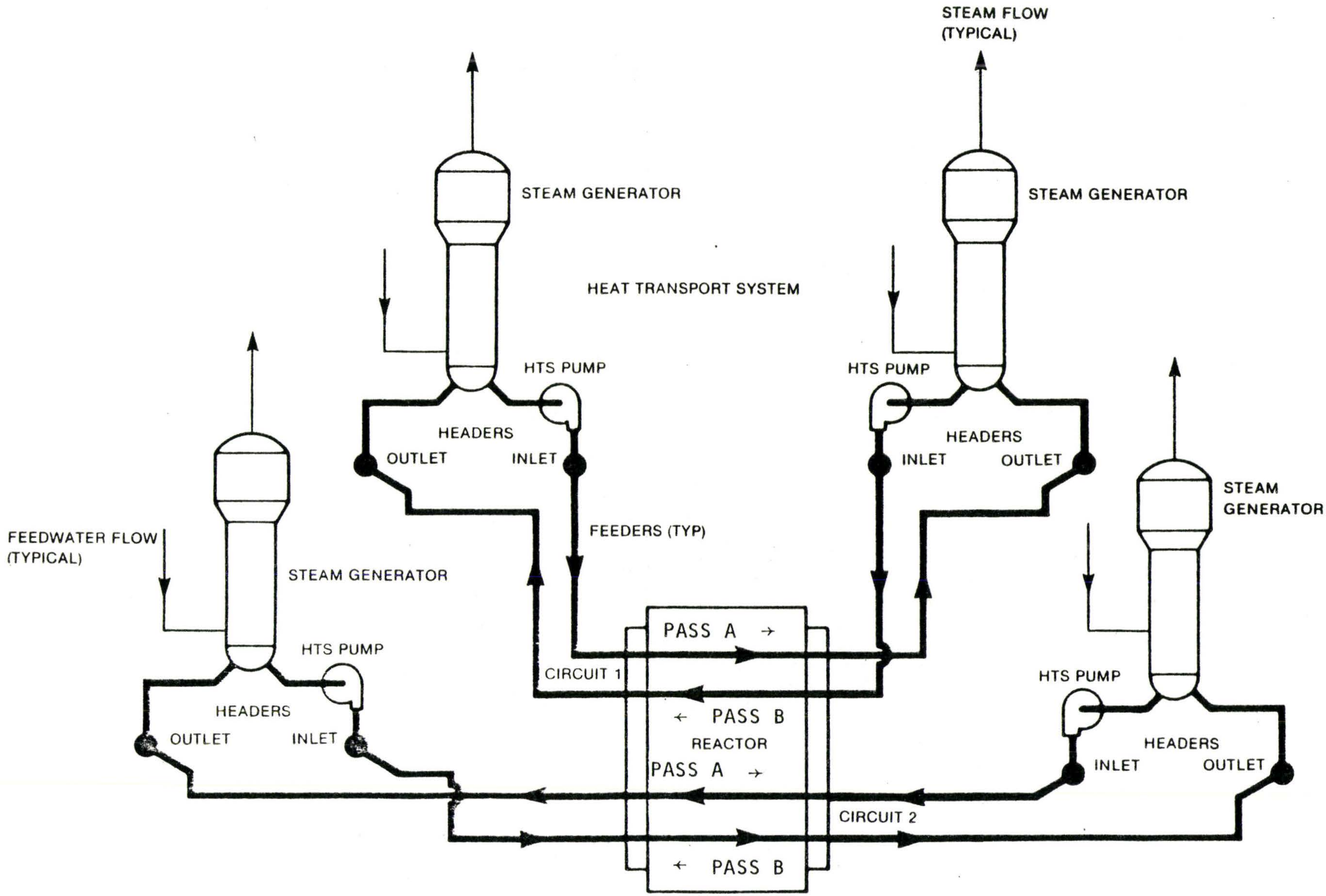

FIGURE 2.3 HEAT TRANSPORT SYSTEM FLOWSHEET

(2) Inlet headers. The inlet headers are used to both equalize and maintain a constant pressure head through the fuel channels. Two sets of breaks are simulated for these headers: inner zone (Figure 2.3), referring to channels in the central region of the core, and outer zone, referring to the outer channels. As with the pump suction break, these are modelled assuming a hole in the structure. A 30% Inlet Header (Inner Zone) break is modelled as a hole of 0.6 times the cross-sectional area of the pipe feeding the inner zone channels.

(3) Outlet header. The outlet headers, like the inlet headers, maintain and equalize the pressure head of the coolant flowing out of the reactor. Again, as with the reactor inlet headers, these are modelled in accident analysis, as disruptions in the coolant flow of either of the two thermalhydraulic zones, e.g., 25% Reactor Outlet Header (Inner Zone) [25% ROH(IZ)].

2.3 Reactor Shutdown Systems

Fast reactor shutdown is achieved with the use of neutron absorbing devices to suppress reactivity. These devices are designed on the basis of their ability to shutdown the reactor adequately when various postulated accidents occur. For the purposes of designing the shutdown systems, this accident is assumed to be a major rupture in the primary heat transport system resulting in a loss of coolant. Though such an accident is highly improbable, the criteria ensure an overall high degree of safety in the shutdown system design.

In CANDU, the shutdown devices are shutoff rods and liquid poison injection nozzles.

2.3.1 Shutoff Rods

In this report, the reactor models used had 2 banks of 15 shutoff rods each (Figure 2.5). The absorber element in each rod was a tube comprised of a stainless steel-cadmium-stainless steel sandwich. The rods fall through a vertical guide tube under gravity. To minimize the time required for the rods to reach the core centreline, a recently developed drive mechanism employing an acceleration spring assists the entry of shutoff rods into the core. As this project will show, the power pulse following loss-of-coolant accidents is strongly dependent on the initial time of entry of the shutoff rod banks into the reactor.

In transient analyses, the two most effective shutoff rods are assumed inoperative to simulate a worst-case scenario. The remaining 28 rods have a total reactivity worth of approximately -80 mk fully inserted. The rods are activated by a triplicated logic system constantly monitoring reactor power. During operation the system is independent of the regulation and process systems. Upon sensing the requirement for a reactor trip, the system de-energizes the direct current clutches on the rods, releasing them. Thus, in the event of a station power failure where the direct current clutches fail or shut off, the rods are automatically sent into the core.

2.3.2 Moderator Poison

The second shutdown system studied was the rapid injection of concentrated gadolinium nitrate solution into the bulk moderator

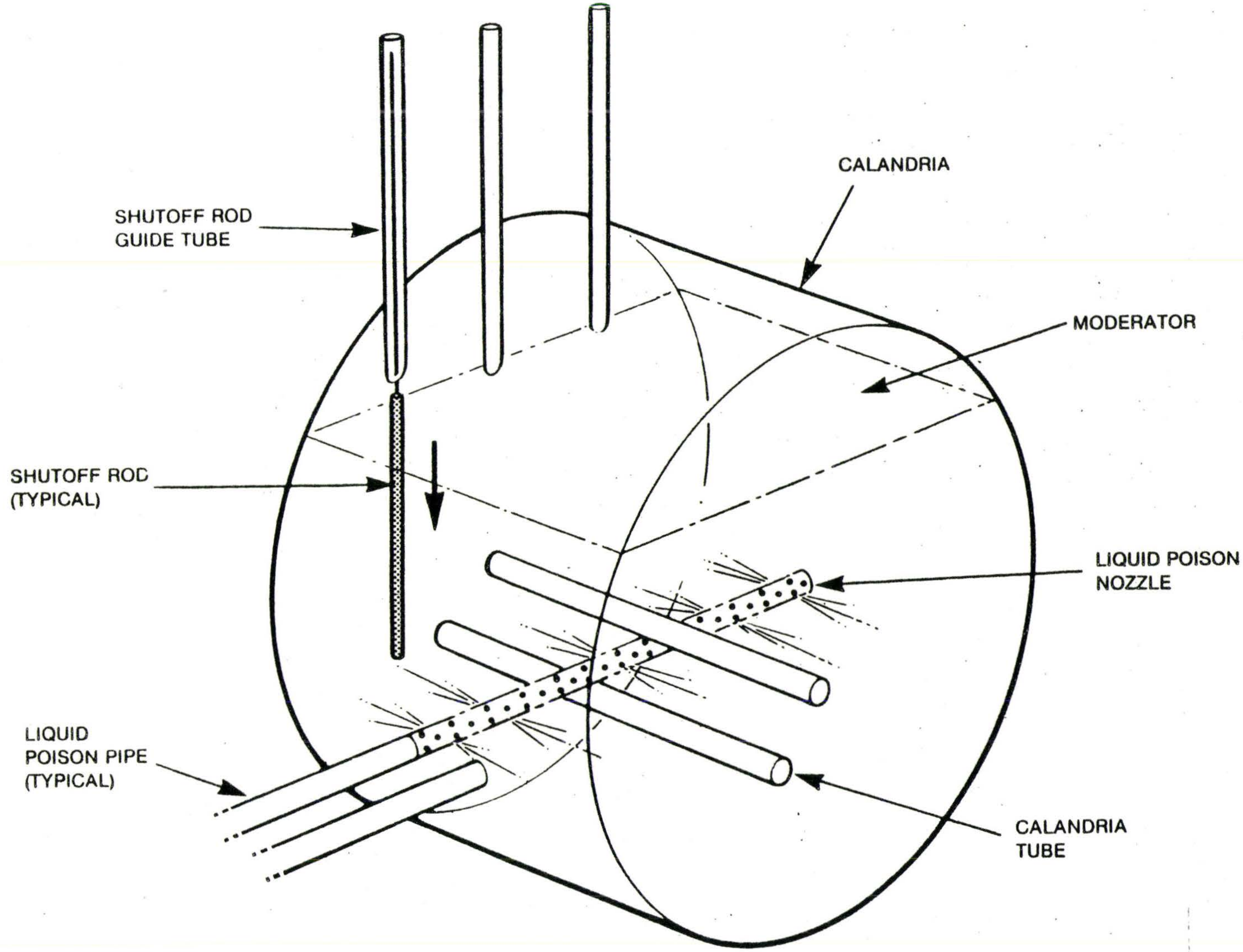

FIGURE 2.4 SHUTDOWN SYSTEMS: SHUTOFF RODS AND LIQUID "POISON" INJECTION

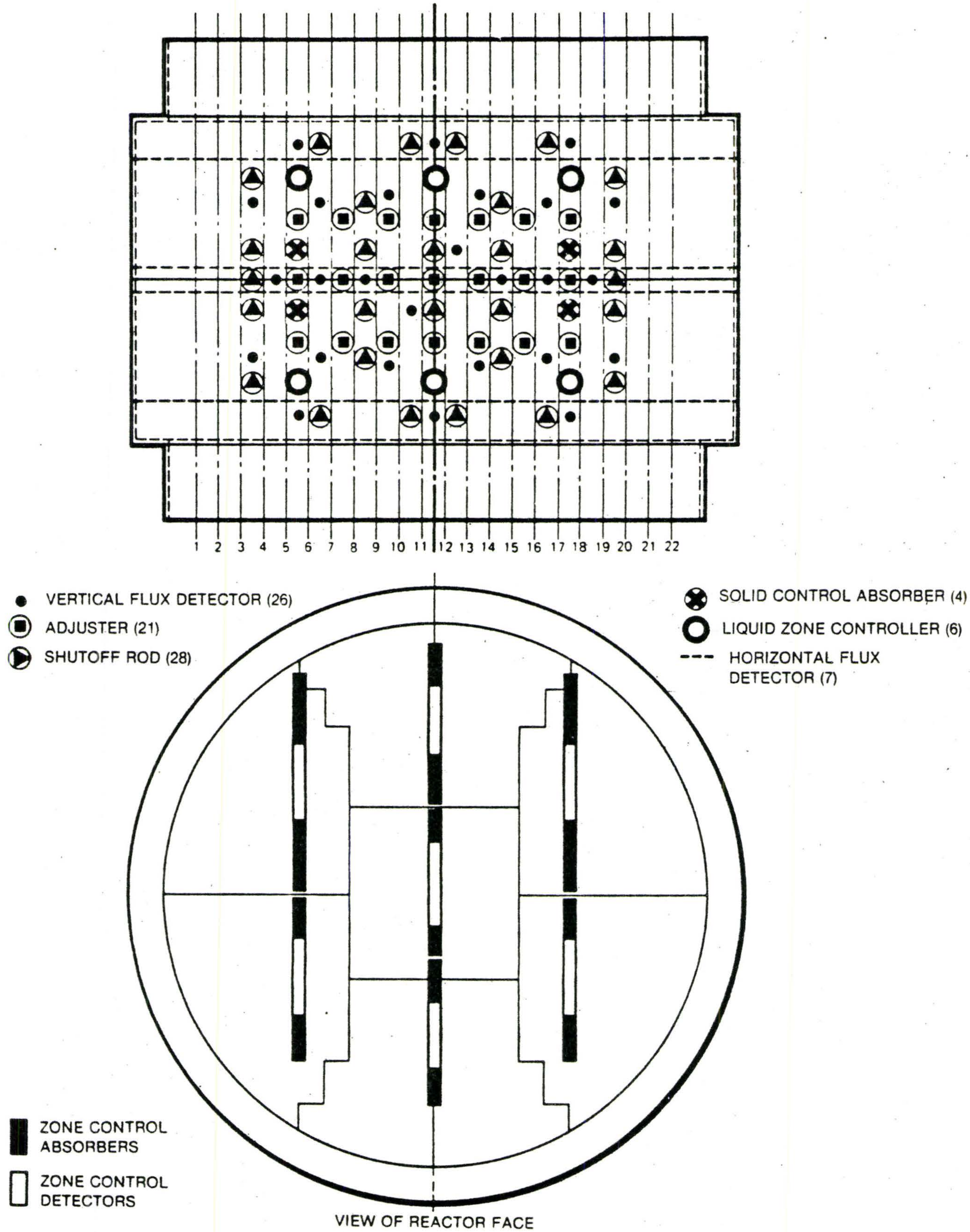

FIGURE 2.5 REACTIVITY MECHANISM LAYOUT

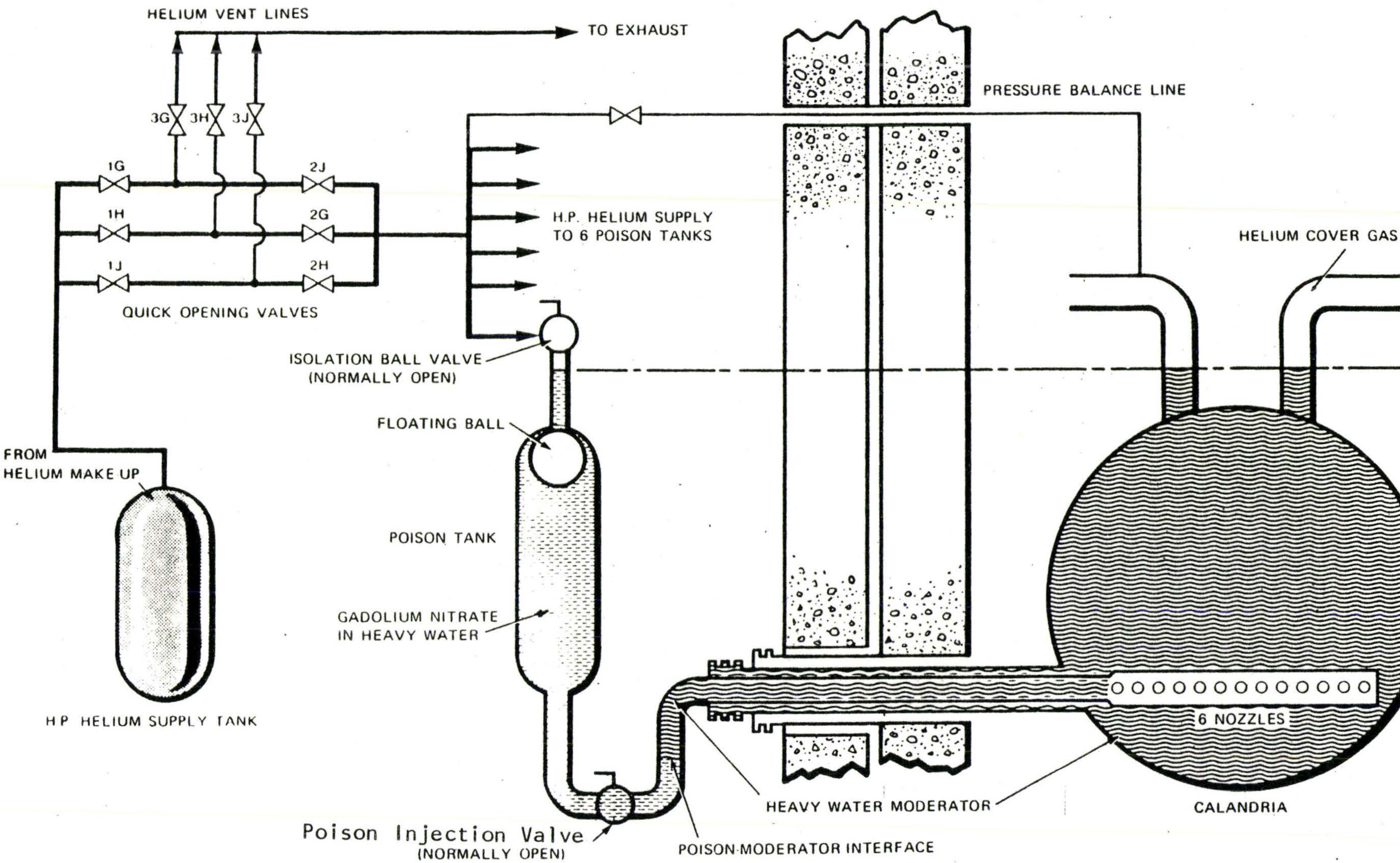

FIGURE 2.6 SCHEMATIC OF SECOND SHUTDOWN SYSTEM

(Figures 2.4 and 2.6). This is achieved by employing a second independent triplicated logic system to sense the requirement for emergency shutdown, and using helium pressure valves to inject the gadolinium poison. Analysis has indicated that within 2 seconds of the injection values opening, 30 mk of negative reactivity is introduced. Eventual dispersal of the gadolinium poison in the moderator will result in a negative reactivity of approximately 300 mk. Subsequent to shutdown, an ion exchange system is used to remove the poison before start-up action begins.

As with the shutoff rods, power is required to maintain the poison injection valves in a closed or off position. Station power failure results in the valves springing open and the rapid subsequent poisoning out of the reactor core.

CHAPTER 3

CANDU DYNAMIC CHARACTERISTICS

3.1 Reactivity Effect of Delayed Neutron Source

Due to the combined effect of dynamic reactivity contributions from the loss of coolant, the operation of the shutdown system, and the presence of a large delayed neutron source, most of the transients encountered in the analysis of CANDU systems are prompt sub-critical, i.e.,

$\rho < \beta$

ρ = dynamic system reactivity

β = total delayed source fraction.

The presence of this large post-event delayed neutron source has a significant effect on the shape, amplitude and time-scale of the neutron transients studied.

In most transients encountered in CANDU analysis, the production of precursors during the transient is small compared to the steady state precursor concentration. Hence, the shape of the pre-event delayed source and the prompt source during the transient account for most of the spatial flux form during the transient. This also results in a significant retardation of the power shape transient, since sub-critical multiplication of the delayed source has a significant effect on the overall system power shape. This results in the amplitude of the power being strongly dependent on the delayed neutron fraction. This effect can be illustrated by considering the contribution of one part of the delayed source, i.e., photoneutrons. Deuterium undergoes a photo disintegration with a 2.24 MeV threshold:

$$\gamma + d \rightarrow n + p.$$

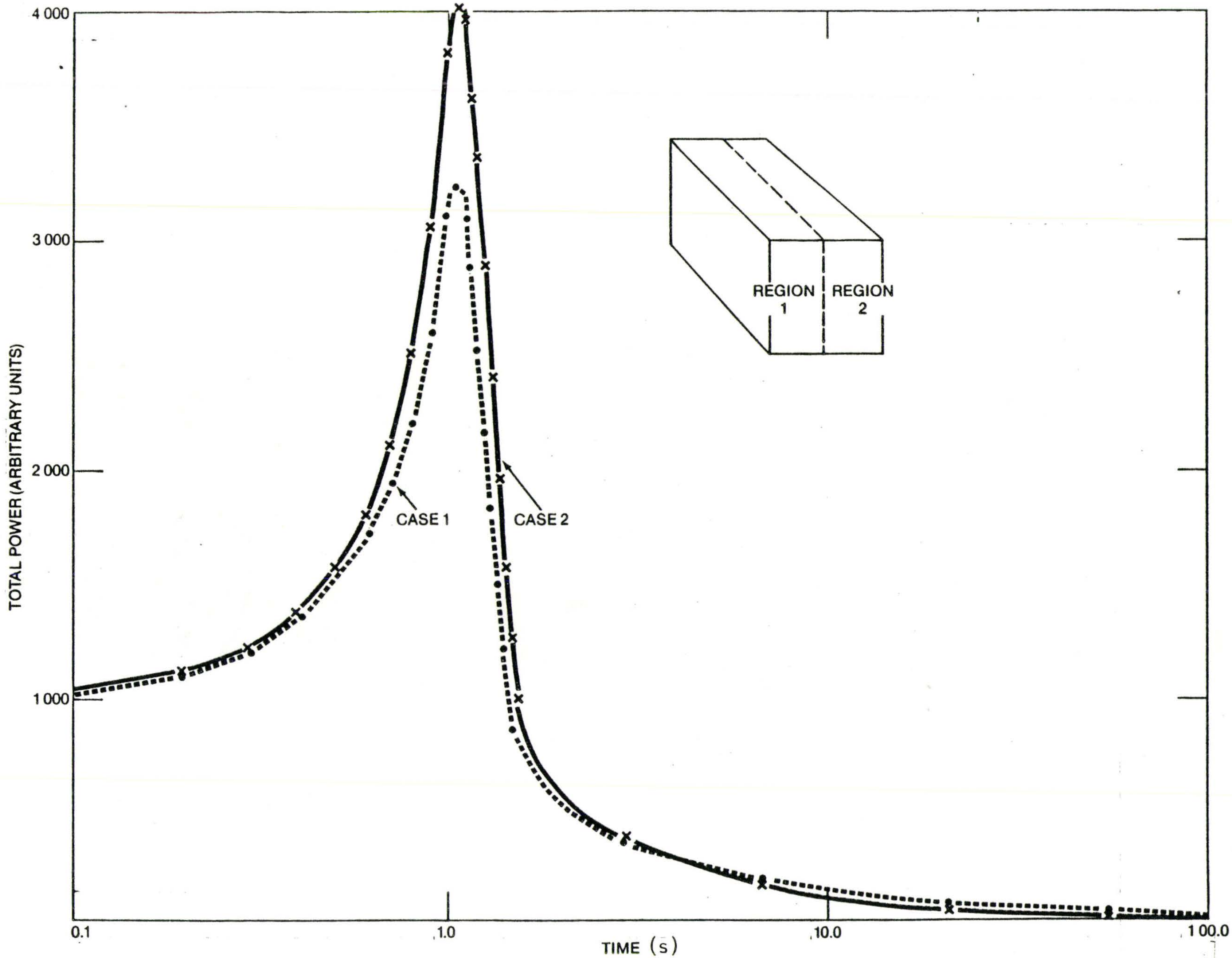

FIGURE 3.1 EFFECT OF PHOTONEUTRONS ON POWER PULSE (REFERENCE 2)

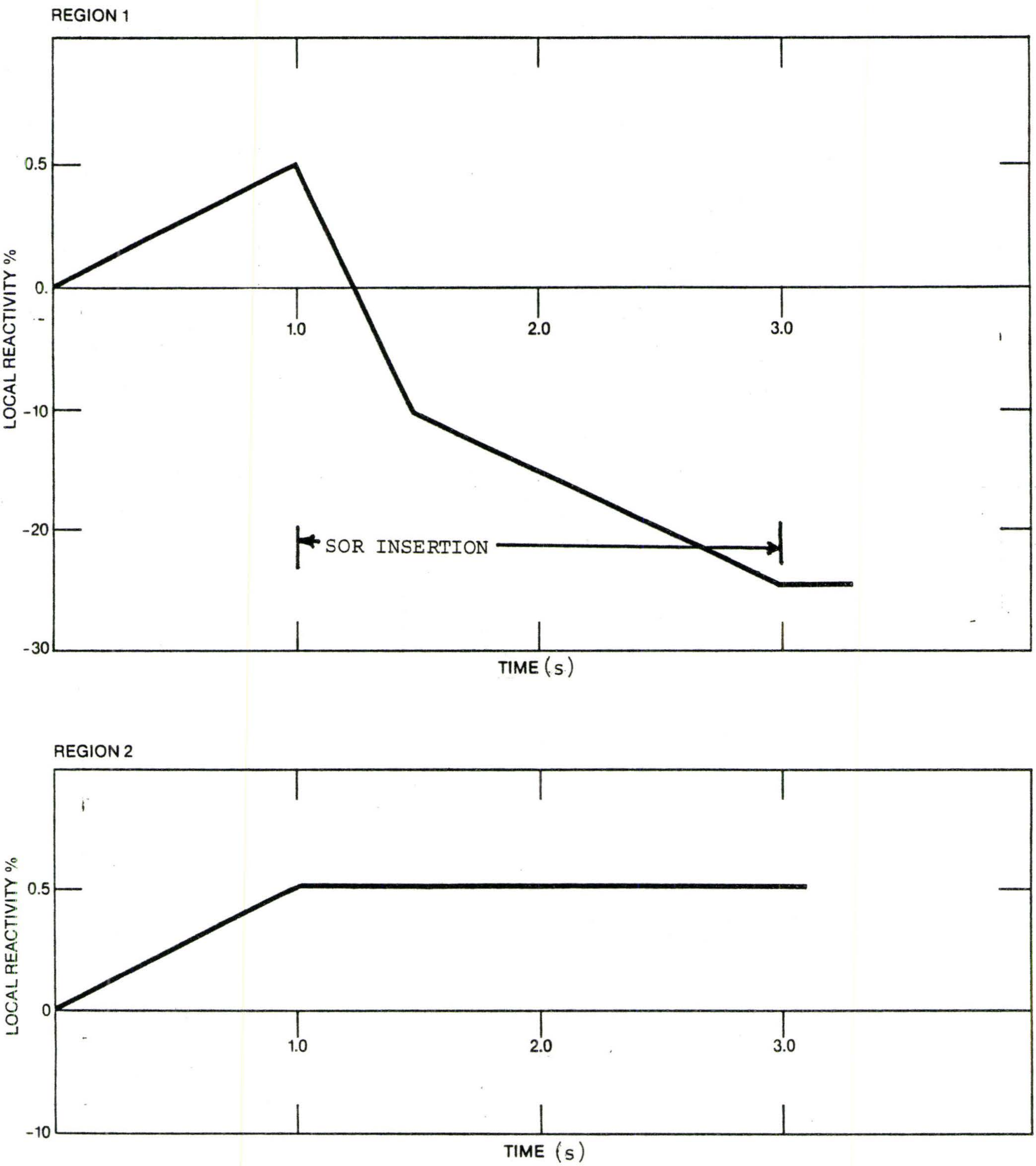

FIGURE 3.2 **APPLIED REACTIVITY TRANSIENTS** (REFERENCE 2)

TABLE 3.1

DELAYED NEUTRON DATA FOR PHOTONEUTRON STUDIES

PHOTONEUTRONS INCLUDED CASE 1		NO PHOTONEUTRONS CASE 2	
λ (s^{-1})	β	λ (s^{-1})	β
0.0137856	0.00072662	0.0125658	0.00012061
0.0305098	0.000819557	0.0305098	0.00111468
0.1336881	0.001041405	0.1336881	0.000967182
0.3155434	0.00233520	0.3164535	0.00167378
1.225077	0.000579031	1.225077	0.000617386
3.147497	0.000225563	3.147497	0.000230924
TOTAL β =	0.00572738	TOTAL β =	0.00472456

It has been found that 17% of the delayed source in CANDU systems is due to photoneutron production in heavy water during operation. To study the significance of the contribution of these photoneutrons to CANDU space-time kinetics, a 3-D model of a CANDU system was set up[2]. Transients following LOCA and the subsequent insertion of shutdown devices were calculated for two cases: one with photoneutrons and one without [Table 3.1]. The 3-D model consisted of two regions (Figure 3.1), with the coolant voiding in both regions. In region 1, shutoff rods were inserted one second after voiding begins. The effect of this on reactivity is shown in Figure 3.2.

Six delayed neutron groups were used in each case, with the effect of photoneutrons included in case 2. Power pulses calculated with and without the photoneutron source are shown in Figure 3.1. The difference of 25% in the peak powers shows the significance of their contribution, and hence the contribution of any delayed source fraction, to the neutron power transient.

3.2 Reactivity Effects Due to Loss of Coolant

If a CANDU reactor experiences a loss of coolant, the net neutronic effect will be an increase in the overall system reactivity. Although the voiding of coolant tends to decrease the thermal fission rate as a result of loss of downscatter from the fast energy group, the resonance absorption is also decreased due to hardening of the flux in the fuel pin cluster. The loss of coolant within the fuel cluster tends to slow fewer fission neutrons down through the resonance region just as they leave the fuel, and hence this decreases the flux of resonance neutrons within the cluster. This results in a positive void reactivity for the coolant.

The reactivity change due to a loss of coolant decreases with fuel irradiation. When coolant is present, an increase in its temperature tends to harden the thermal neutron spectrum, and this is a positive reactivity effect if plutonium is present in the fuel. As coolant is lost, this hardening effect no longer occurs. This results in a decrease in reactivity, its magnitude dependent on the uranium-plutonium isotope ratios in the fuel. The latter depends on the degree of fuel irradiation.

CHAPTER 4

CANDU LATTICE PHYSICS CHARACTERISTICS

Various neutronic features of the CANDU reactor system provide the basis for the method of analysis of neutron power transients. These include:

4.1 High Scattering to Absorption Ratio

In the CANDU system, the use of deuterium as both a moderator and a coolant results in a high scattering/absorption ratio in the core region, and consequently leads to a long thermal diffusion length. This implies that Fick's Law is a valid approximation for use in the CANDU system, and experiment and analysis have supported this conclusion. Hence, diffusion theory is used in the solution of neutron kinetics transients. This eliminates the difficulties and restrictions of using transport theory codes and allows larger and more detailed models to be studied.

4.2 Sufficiency of One or Two Neutron Groups

With any diffusion theory calculation, the complexity of the solution is dependent on the number of energy groups which the neutron flux must be broken up into. Pressurized heavy water reactor kinetics has been excellently modelled using only one or two energy groups in a neutron transient calculation. This is due to the extremely high thermalization of the neutron flux in a CANDU system. Figure 4.1 illustrates this point. Studies have shown that over 95% of the neutrons in the moderator in a CANDU lattice are thermalized. Thus, one or two neutron groups are sufficient to model most reactor transients.

	LIGHT WATER	HEAVY WATER	GRAPHITE
SLOWING DOWN POWER CM^{-1}	1.35	0.178	0.06
MODERATING RATIO	60	2,000	170
NEUTRON WASTAGE IN MODERATOR, COOLANT AND CORE STRUCTURES PER FISSION (TYPICAL)	PWR .28	CANDU PHW .15	MAGNOX 0.16
	BWR .25		AGR 0.3

FIGURE 4.1 MODERATING EFFICIENCY OF HEAVY WATER

CHAPTER 5

TRIP LOGIC

Neutron power level in the reactor is measured by an assembly of flux detectors consisting of two types: out of core ion chambers and in-core self-powered detectors. Detector outputs are monitored by a trip logic circuit. There are both neutronic and process system trip set points in the trip logic system. The neutronic trip set points are:

a) high neutron power trip - if the reactor exceeds a maximum allowable local power limit (e.g., 110% of licensed full power), the reactor is tripped.

b) high rate neutron power trip - if the rate of increase in reactor power exceeds a maximum allowable local limit, the reactor is tripped. The ion chambers monitor $d\frac{\ln \phi}{dt} = \frac{d\phi}{\phi dt} \approx \frac{\Delta\phi}{\phi\Delta t}$ for this trip condition. A 10%/sec rise will trip Shutdown System #1 (Shutoff rods) and a more serious power excursion of 25%/sec or greater will trigger Shutdown System #2 (poison injection) trip.

c) high log neutron power trip - this trip level is used when a low core coolant flow trip is conditioned out. This would occur when the reactor is at a low power and low coolant flow level, for example during maintenance or shut-down cooling. Again, this is monitored by the ion chambers, and is activated whenever $\ln \phi$ exceeds the allowable set point.

The detector networks are divided into 3 trip channels in the reactor. Tripping of any one detector in a channel triggers a channel trip, and the tripping of two channels triggers a whole reactor trip involving the shutdown system. This system of trip logic is termed "2 out of 3 coincidence". This is used to ensure a high level of system reliability and availability. For example, if a sensor or trip channel were to fail (i.e., not provide a trip signal when a trip set point is reached), the remaining two trip channels would continue to provide protection. On the other hand, if a sensor were to fail "positive" (i.e., provide a spurious trip signal), the 2-signal aspect would prevent a spurious reactor trip. Two out of three coincidence also allows a detector or trip channel to be tested without causing either a reactor trip or leaving the reactor fully unprotected.

To ensure that the results obtained from simulations are on the conservative side, the following assumptions are made:

1) the first detector trip per trip channel is not recorded. This delays the implementation of the shutdown systems, allowing the transient to proceed further before action is taken.
2) the first trip channel to trip is ignored. Again, this allows the system to proceed before the shutdown devices are activated.

In the simulation, two forms of instrument delays are accounted for. The first is the instrument response delay introduced by the electronics of the trip logic system; the second is the mechanical delay of the movement or activation of the shutdown systems after receiving an activation signal.

CHAPTER 6

COMPUTATIONAL ANALYSIS

6.1 Dependence of Power Pulses on Delay Time and Rod Drop

An initial study was done to demonstrate the effect of the rate of shutoff rod insertion on neutronic power pulses following a breach in the primary cooling system. A 3-dimensional CANDU reactor model was set up. Using the point kinetics method, power pulses following a 40% Inlet Header Break were calculated for various shutoff rod drop curves. A standard bank of 28 instead of 30 shutoff rods was used (See Chapter 2.3.1), again, the two most effective rods assumed inoperative for a more conservative margin. The time delay between when the break occurred and when the de-energization of the direct current clutches holding the shutoff rods occurred was assumed to be 0.4 seconds. This is consistent with actual measurements of the response system.

The rod entry in three of the cases was assisted by an acceleration spring drive mechanism. Three different spring actions were studied:

1) Slow rod case - no spring extension,
2) Type B - 71 cm spring extension with light element 18.1 kg (40 lb) and 1780N acceleration,
3) Type C - 142 cm spring extension with light element 18.1 kg (40 lb) and 1780N acceleration,
4) Type D - 183 cm spring extension with light element 18.1 kg (40 lb) and 1780N acceleration.

Figure 6.1 shows the different drop curves used in the simulation.

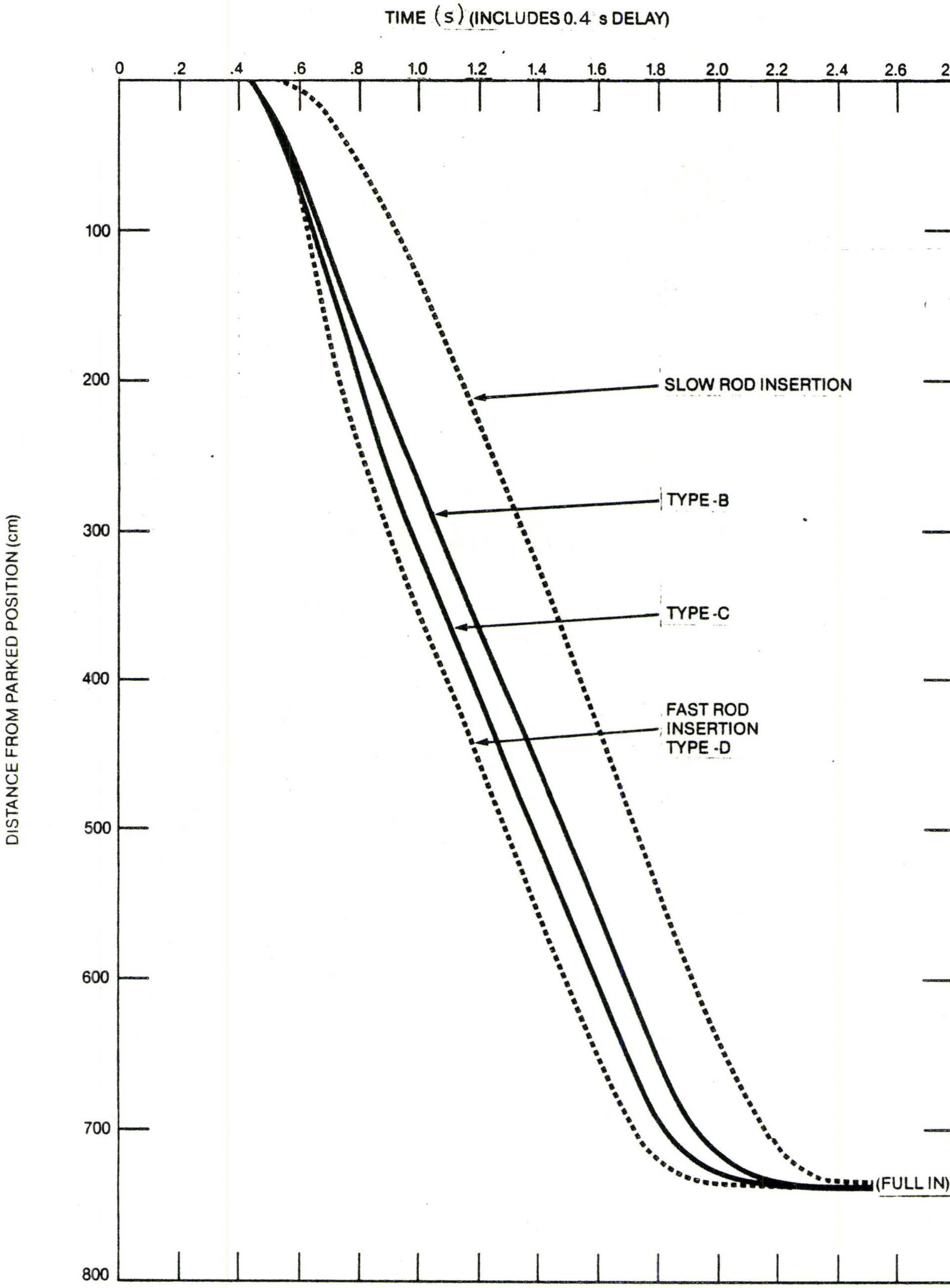

FIGURE 6.1 SOR DISPLACEMENT vs TIME AFTER INLET HEADER BREAK

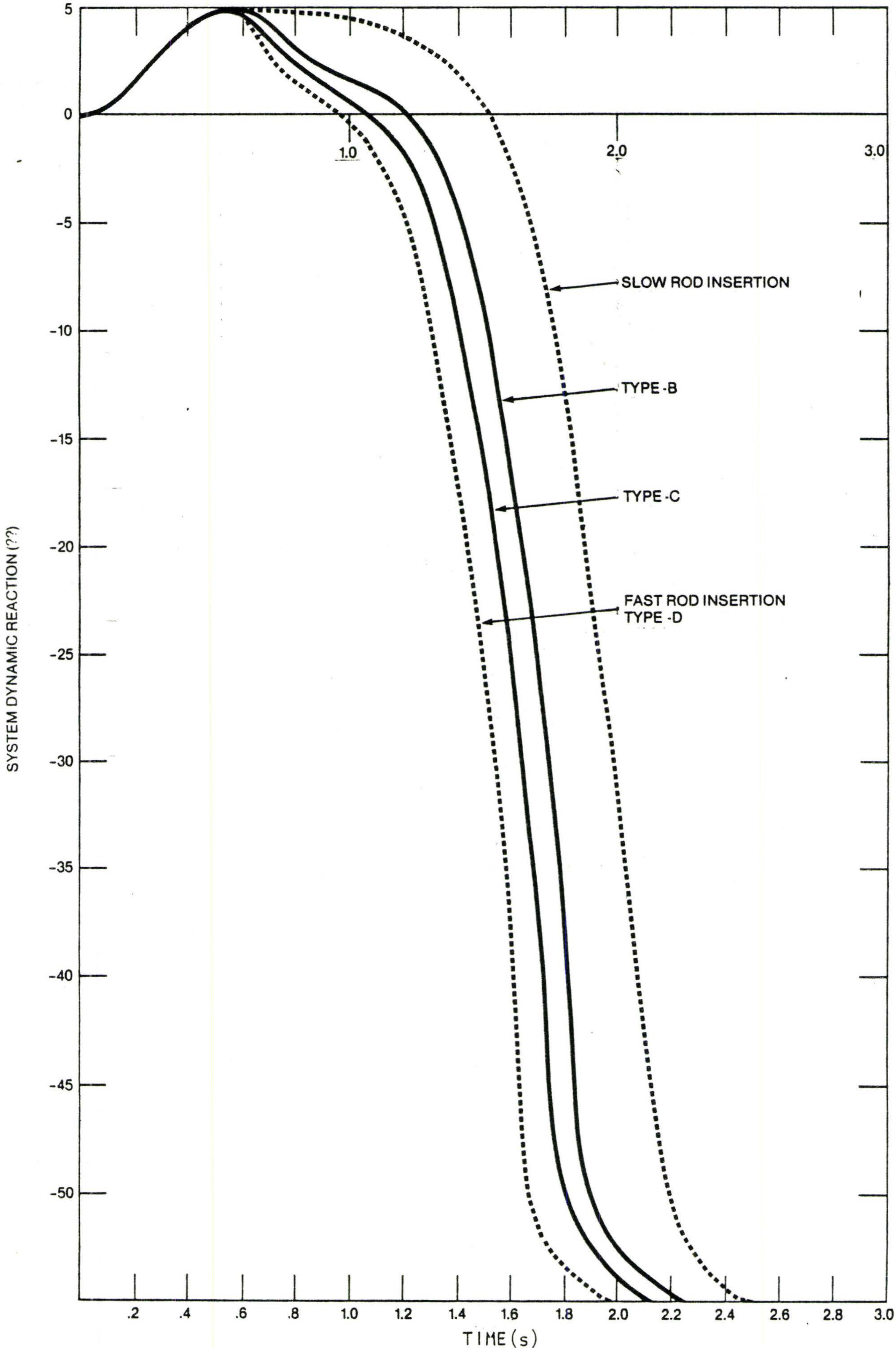
SLOW ROD INSERTION
TYPE -B
TYPE -C
FAST ROD INSERTION
TYPE -D
SYSTEM DYNAMIC REACTION (??)
TIME (s)
5
0
-5
-10
-15
-20
-25
-30
-35
-40
-45
-50
.2
.4
.6
.8
1.0
1.2
1.4
1.6
1.8
2.0
2.2
2.4
2.6
2.8
3.0

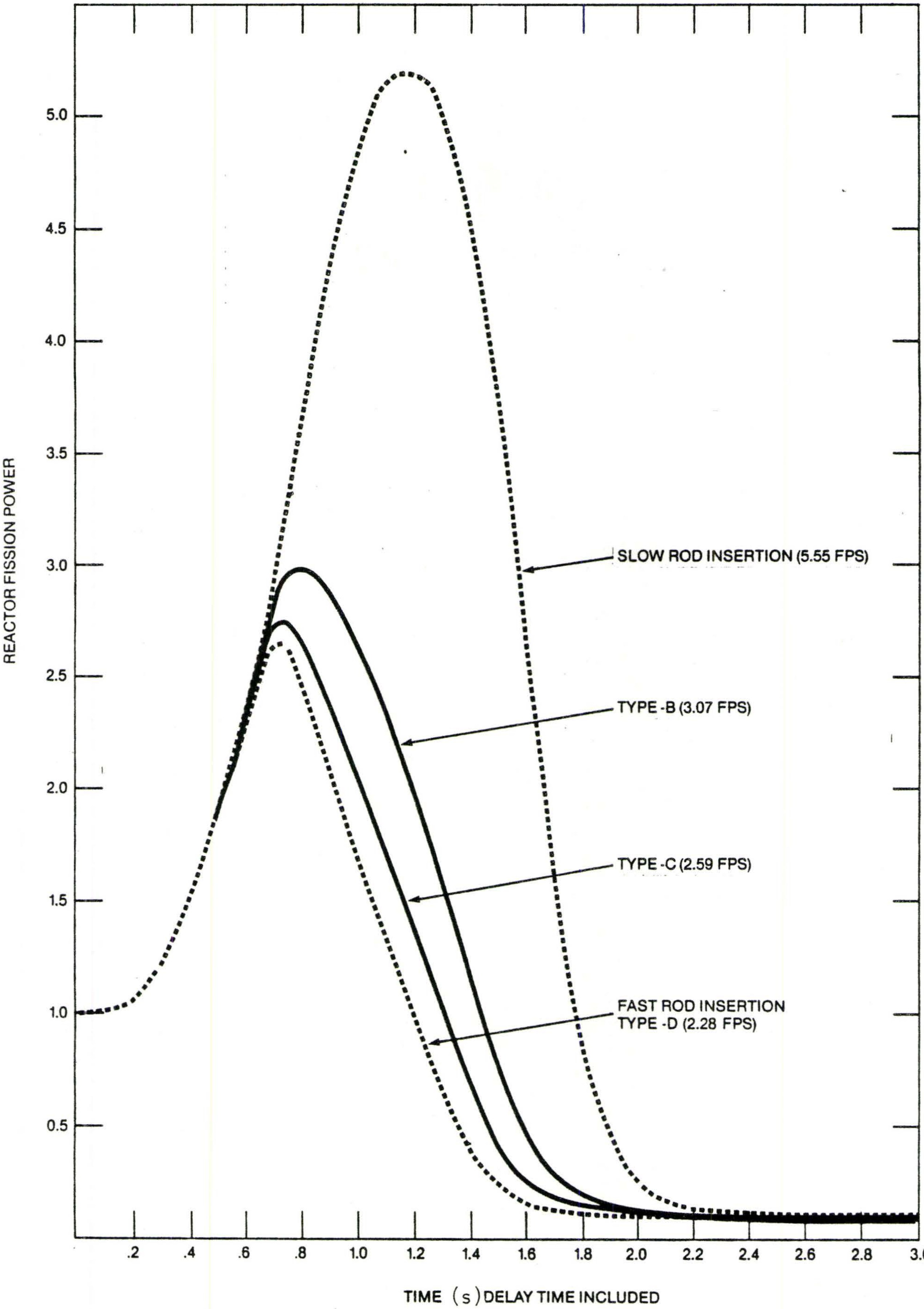

5.0
4.5
4.0
3.5
3.0
2.5
2.0
1.5
1.0
0.5
REACTOR FISSION POWER
SLOW ROD INSERTION (5.55 FPS)
TYPE -B (3.07 FPS)
TYPE -C (2.59 FPS)
FAST ROD INSERTION
TYPE -D (2.28 FPS)
.2
.4
.6
.8
1.0
1.2
1.4
1.6
1.8
2.0
2.2
2.4
2.6
2.8
3.0
TIME (s) DELAY TIME INCLUDED

TABLE 6.1.1 - PARAMETERS FOR SLOW AND FAST ROD CASES

Time	Fractional Change in Coolant Density d	Dynamic Void Reactivity mk	Elevation of Slow Rod (cm)	Dynamic ROD Reactivity (slow) mk	Dynamic System Reactivity Slow Rod Case ρ_s	Elevation of Fast Rod (cm)	Dynamic Rod Reactivity (fast) mk	Dynamic System Reactivity Fast Rod Case ρ_f	Reactor Fission Power: Slow Rod Case	Reactor Fission Power: Fast Rod Case
0.07	0.0	0.0	0.0	0.0	0.0	0.0	0.0	0.0	1.000	1.000
0.12	0.023	0.306	0.0	0.0	0.306	0.0	0.0	0.306	1.007	1.007
0.22	0.118	1.459	0.0	0.0	1.459	0.0	0.0	1.459	1.088	1.088
0.35	0.275	3.475	0.0	0.0	3.475	0.0	0.0	3.475	1.366	1.366
0.40	0.319	4.059	0.0	0.0	4.059	0.0	0.0	4.059	1.536	1.536
0.50	0.372	4.432	0.0	0.0	4.432	12.1	0.0	4.432	1.920	1.920
0.60	0.398	5.187	9.14	0.0	5.187	76.2	-0.2	4.987	2.398	2.373
0.70	0.405	5.331	30.48	0.0	5.331	173.7	-2.1	3.231	2.998	2.629
0.80	0.412	5.447	60.96	-0.1	5.347	252.9	-3.7	1.747	3.622	2.455
0.90	0.428	5.709	97.54	-0.532	5.177	310.8	-5.0	0.709	4.254	2.093
1.03	0.460	6.136	146.3	-1.511	4.624	374.9	-6.9	-0.764	4.889	1.593
1.10	0.490	6.536	182.8	-2.215	4.321	408.4	-8.2	-1.664	5.094	1.351
1.16	0.516	6.883	210.3	-2.280	4.003	441.9	-9.9	-3.017	5.180	1.148
1.22	0.540	7.203	237.7	-3.462	3.741	469.3	-11.5	-4.297	5.187	0.956
1.28	0.560	7.470	268.2	-4.059	3.411	499.8	-14.0	-6.53	5.119	0.773
1.34	0.574	7.657	301.7	-4.705	2.952	530.3	-17.9	-10.243	4.956	0.587
1.39	0.584	7.790	332.2	-5.485	2.305	557.7	-21.8	-14.01	4.713	0.447
1.45	0.592	7.897	359.6	-6.269	1.628	586.7	-27.0	-19.103	4.303	0.320
1.50	0.595	7.937	390.1	-7.317	0.620	612.6	-31.5	-23.56	3.865	0.251

TABLE 6.1.1 - (CONTINUED)

Time	Fractional Change in Coolant Density d	Dynamic Void Reactivity mk	Elevation of Slow Rod (cm)	Dynamic ROD Reactivity (slow) mk	Dynamic System Reactivity Slow Rod Case ρ_s	Elevation of Fast Rod (cm)	Dynamic Rod Reactivity (fast) mk	Dynamic System Reactivity Fast Rod Case ρ_f	Reactor Fission Power	
									Slow Rod Case	Fast Rod Case
1.55	0.597	7.963	417.5	-8.510	-0.547	637.0	-36.2	-28.24	3.337	0.203
1.60	0.599	7.990	445.0	-9.961	-1.971	664.4	-42.0	-34.01	2.764	0.170
1.65	0.599	7.990	472.4	-11.760	-3.770	691.8	-55.4	-47.41	2.190	0.145
1.70	0.599	7.990	499.8	-14.040	-6.050	713.2	-60.0	-52.01	1.658	0.127
1.75	0.599	7.990	524.2	-17.003	-9.013	728.4	-63.29	-55.3	1.203	0.114
1.81	0.599	7.990	551.6	-20.831	-12.841	728.4	-63.29	-55.3	0.802	0.109
1.86	0.599	7.990	585.2	-26.425	-18.435	728.4	-63.29	-55.3	0.563	0.107
1.99	0.605	8.070	652.0	-39.479	-31.409	728.4	-63.29	-55.22	0.277	0.103
2.05	0.612	8.164	673.6	-51.644	-43.480	728.4	-63.29	-55.12	0.204	0.101
2.50	0.640	8.537	728.4	-63.297	-54.760	728.4	-63.29	-54.75	0.126	0.091

TABLE 6.1.2 - PARAMETERS FOR CASES B AND C

Time (sec)	Fractional Change in Coolant Density (d)	Dynamic Void Reactivity (mk)	Elevation of Rods (cm)		Dynamic Rod Reactivity (mk)		Dynamic System Reactivity (ρ)		Reactor Fission Power	
			Type-B	Type-C	Type-B	Type-C	Type-B	Type-C	Type-B	Type-C
0.07	0.0	0.0	0.0	0.0	0.0	0.0	0.0	0.0	1.000	1.000
0.12	0.023	0.306	0.0	0.0	0.0	0.0	0.306	0.306	1.007	1.007
0.22	0.118	1.459	0.0	0.0	0.0	0.0	1.459	1.459	1.088	1.088
0.35	0.275	3.475	0.0	0.0	0.0	0.0	3.475	3.475	1.366	1.366
0.40	0.319	4.059	0.0	0.0	0.0	0.0	4.059	4.059	1.536	1.536
0.50	0.372	4.432	12.1	12.1	0.0	0.0	4.432	4.432	1.920	1.920
0.60	0.398	5.187	60.9	68.5	-0.1	-0.15	5.087	5.037	2.385	2.379
0.70	0.405	5.331	121.9	152.4	-0.8	-1.6	4.531	3.731	2.839	2.710
0.80	0.412	5.447	173.7	187.5	-2.1	-3.0	3.347	2.447	3.011	2.668
0.90	0.428	5.709	244.0	271.2	-3.15	-4.05	2.559	1.659	2.897	2.414
1.03	0.460	6.136	286.5	333.7	-4.4	-5.5	1.736	0.636	2.568	2.003
1.10	0.490	6.536	320.0	370.3	-5.2	-6.7	1.336	-0.164	2.364	1.768
1.16	0.516	6.883	350.5	399.2	-6.0	-7.9	0.883	-1.017	2.183	1.557
1.22	0.540	7.203	381.0	426.7	-7.0	-9.1	0.203	-1.897	1.983	1.349
1.28	0.560	7.470	411.4	457.2	-8.2	-10.8	-0.73	-3.33	1.757	1.140
1.34	0.574	7.657	438.9	487.6	-9.8	-12.7	-2.143	-5.043	1.498	0.934
1.39	0.584	7.790	466.3	512.0	-11.2	-15.5	-3.41	-7.71	1.265	0.785
1.45	0.592	7.897	493.7	542.5	-13.3	-19.0	-5.403	-11.103	1.008	0.562
1.50	0.595	7.937	518.2	563.8	-16.2	-22.7	-8.263	-14.763	0.798	0.431
1.55	0.597	7.963	542.5	591.3	-19.5	-27.9	-11.537	-19.937	0.605	0.324
1.60	0.599	7.990	566.9	612.6	-23.3	-31.5	-15.31	-23.51	0.452	0.255
1.65	0.599	7.990	591.3	637.0	-27.9	-36.2	-19.91	-28.21	0.340	0.209
1.70	0.599	7.990	617.2	664.4	-32.4	-42.5	-24.41	-34.51	0.265	0.171
1.75	0.599	7.990	643.1	685.8	-36.6	-54.4	-28.61	-46.41	0.218	0.131
1.81	0.599	7.990	670.5	716.2	-45.0	-61.2	-37.01	-53.21	0.170	0.106
1.86	0.599	7.990	694.9	728.4	-58.0	-63.29	-50.01	-55.28	0.128	0.098
1.99	0.605	8.070	728.4	728.4	-63.29	-63.29	-55.22	-55.22	0.103	0.093
2.05	0.612	8.164	728.4	728.4	-63.29	-63.29	-55.13	-55.13	0.100	0.092
2.30	0.640	8.537	728.4	728.4	-63.29	-63.29	-54.76	-54.76	0.100	0.082

In Table 6.1 can be seen the variation in coolant density as a function of time. This leads to the dynamic void reactivity shown in Column 3. The dynamic rod reactivities are shown in Column 5 and 8. The dynamic void reactivity and the dynamic rod reactivity were combined to obtain the dynamic system reactivity (Columns 6 and 9). This information was used in the point kinetics calculations of the power transients. The calculated neutronic power transients are shown in Figure 6.3.

The effect of assisted rod entry is apparent. Even the smallest amount of assist studied was significantly better than the straight gravity drop in reducing the peak and duration of the power pulse. This set of simulations illustrates the importance of the rods "biting" into the pulse early, as the entire transient is strongly dependent on its dynamic reactivity characteristics in the early stages of the transient.

A further set of analyses was carried out. With the same LOCA conditions (40% IHB), a series of transients were calculated for 3 realistic rod drop cases:

Case 1A - Light Element (18.1 kg) with 712N acceleration spring and 183 cm spring extension,

Case 3B - Light Element (18.1 kg) with 1601N acceleration spring and 71 cm spring extension with spring preloaded 100 lbs.

- Standard Element - (45.4 kg) with 445N acceleration spring and 71 cm spring extension.

Five delay times were studied: 0, 0.20, 0.30, 0.40 and 0.50 seconds. A point kinetics code was again used in the simulations. Results for the various shutoff rod types are shown in Figures 6.5 and 6.8.

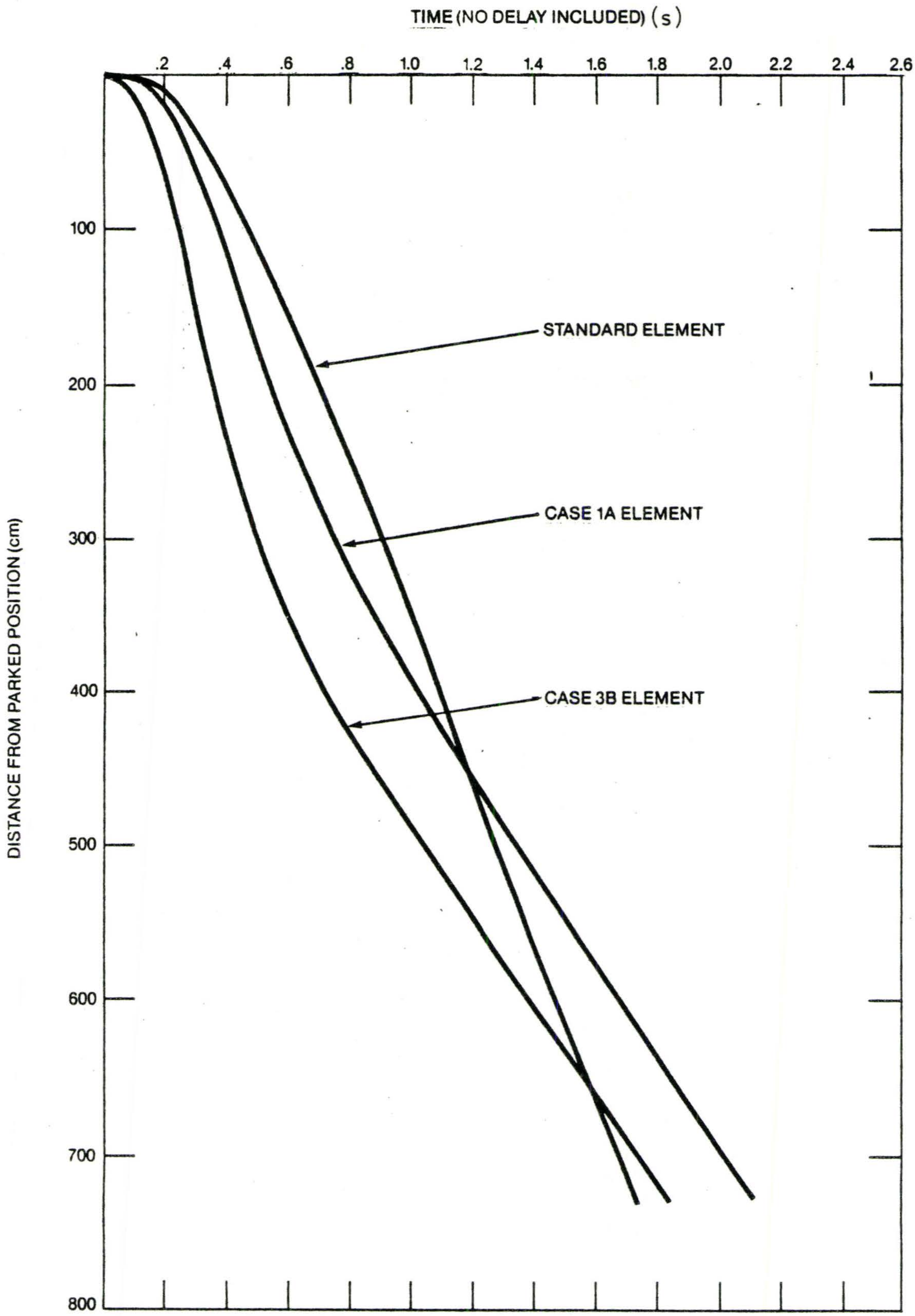

FIGURE 6.4 SOR DISPLACEMENT vs TIME AFTER DE-ENERGIZATION OF CLUTCH

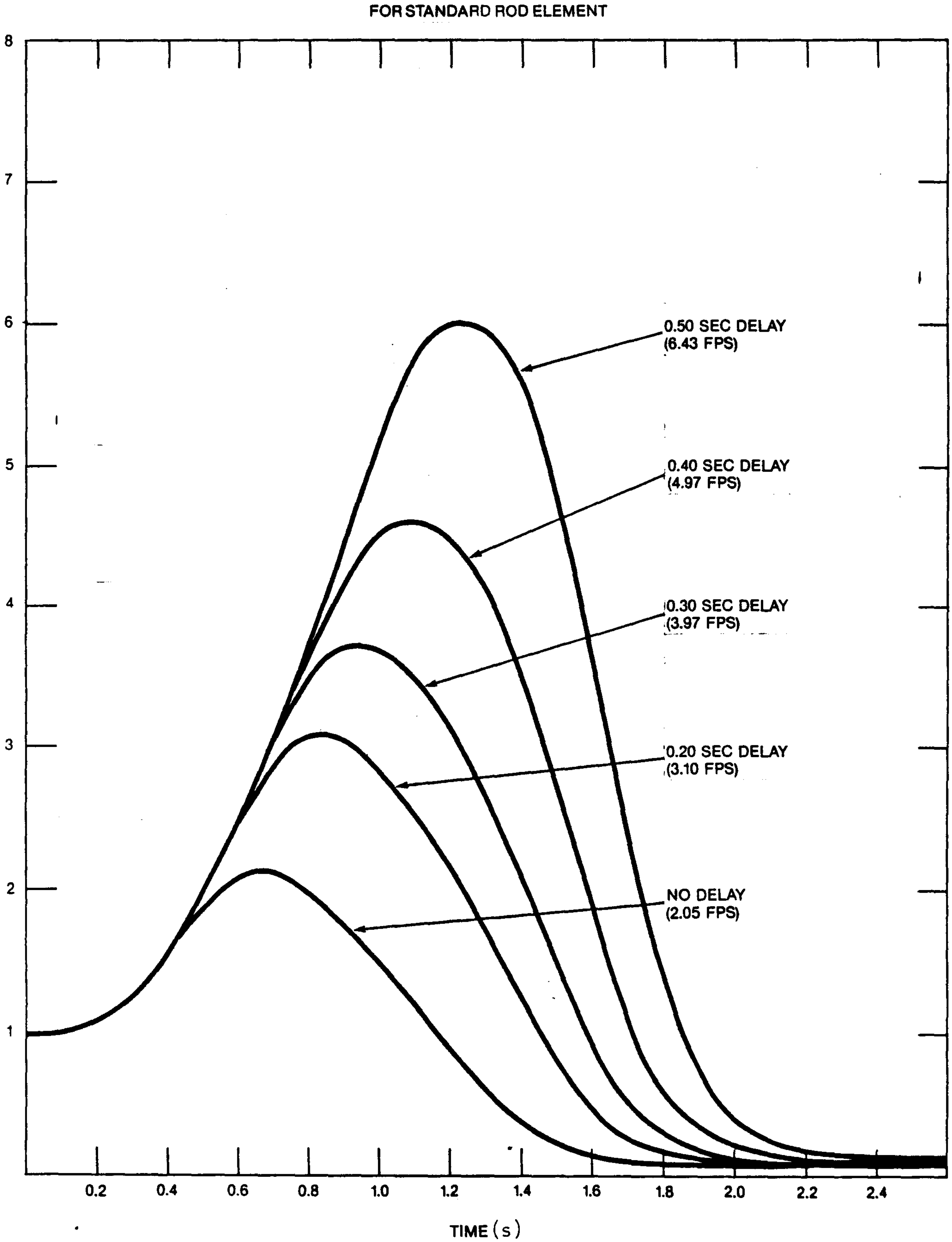

FIGURE 6.5 FISSION POWER AMPLITUDE vs TIME AFTER INLET HEADER BREAK

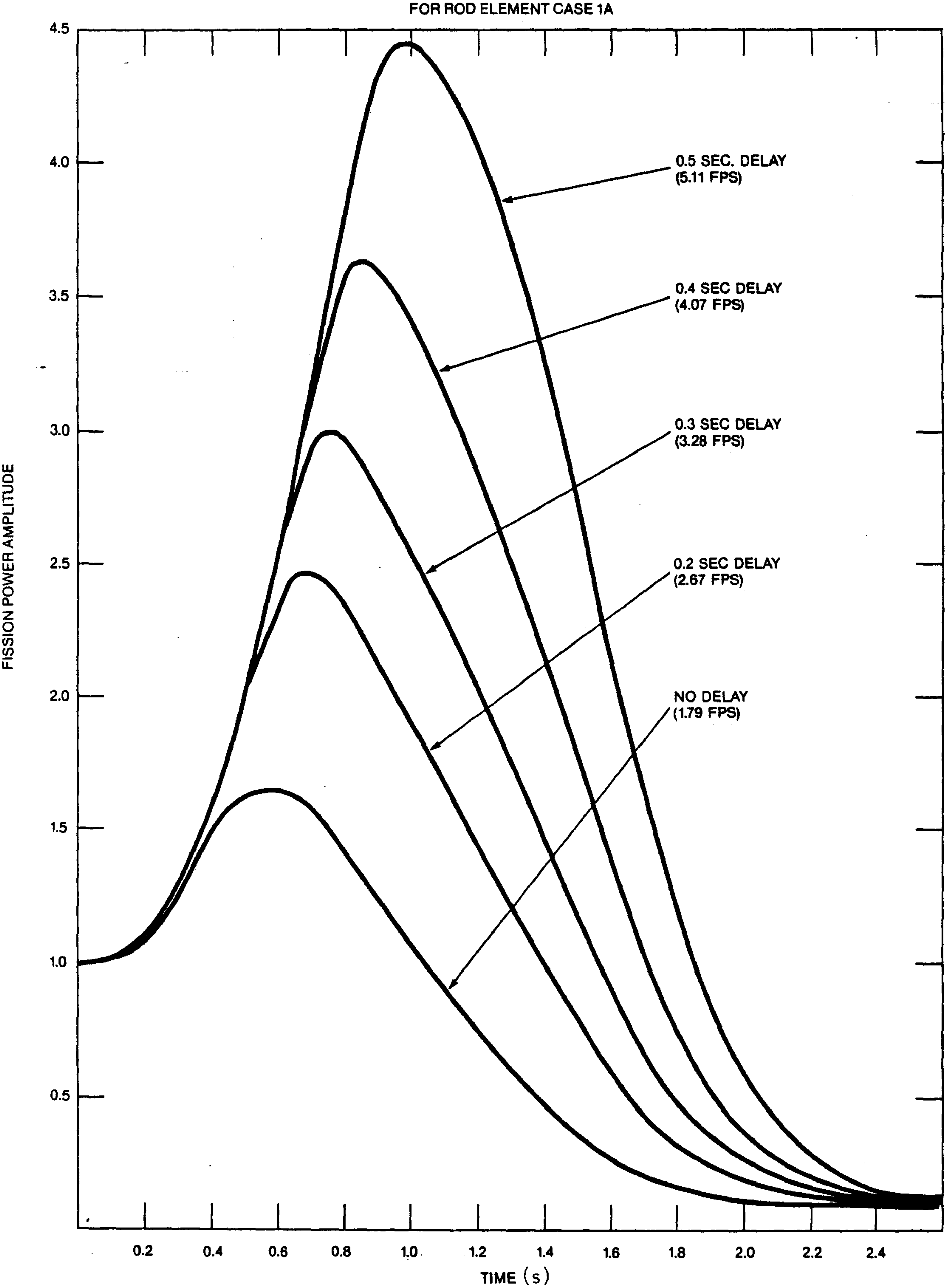

FIGURE 6.6 FISSION POWER AMPLITUDE vs TIME AFTER INLET HEADER BREAK

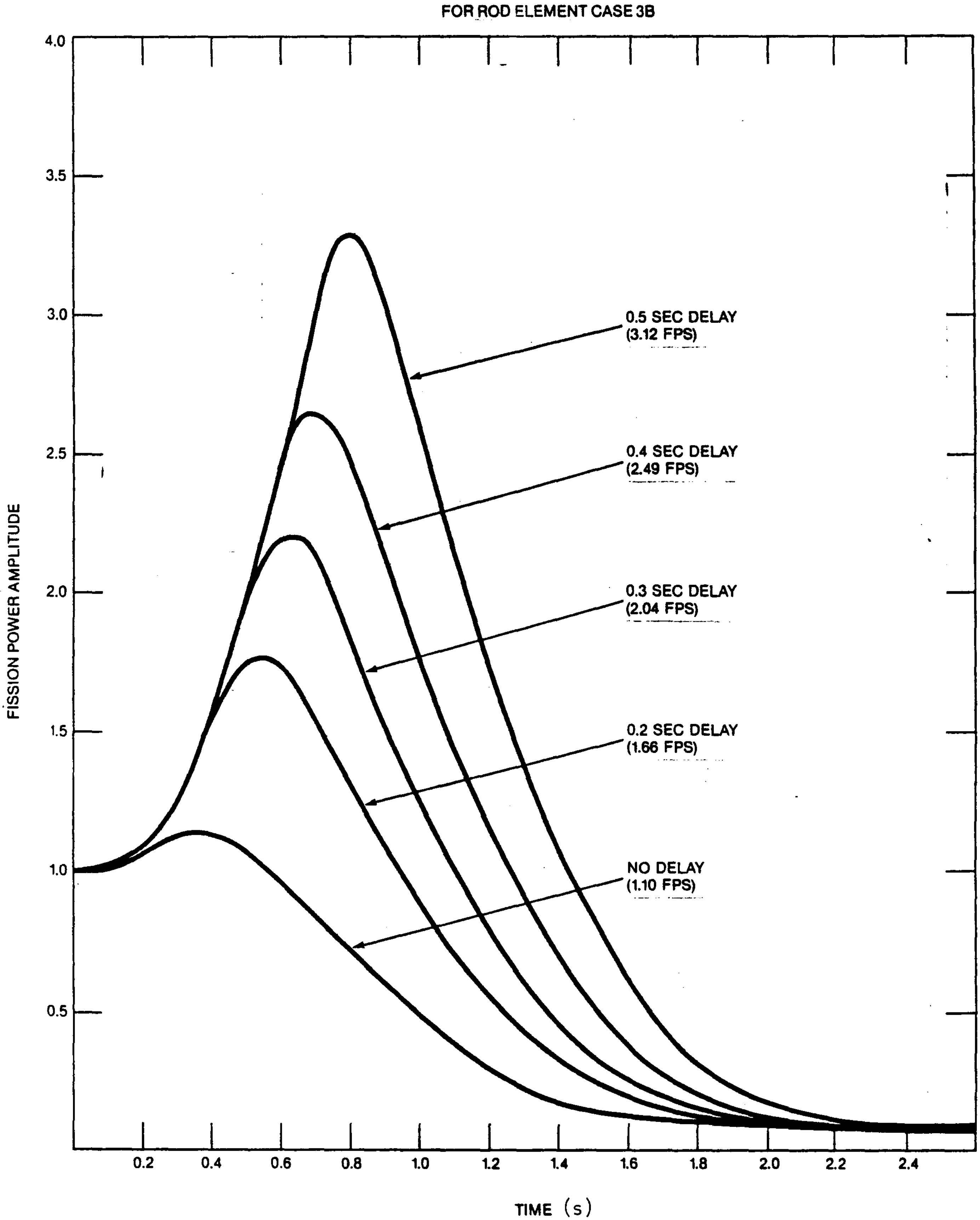

FIGURE 6.7 FISSION POWER AMPLITUDE vs TIME AFTER INLET HEADER BREAK

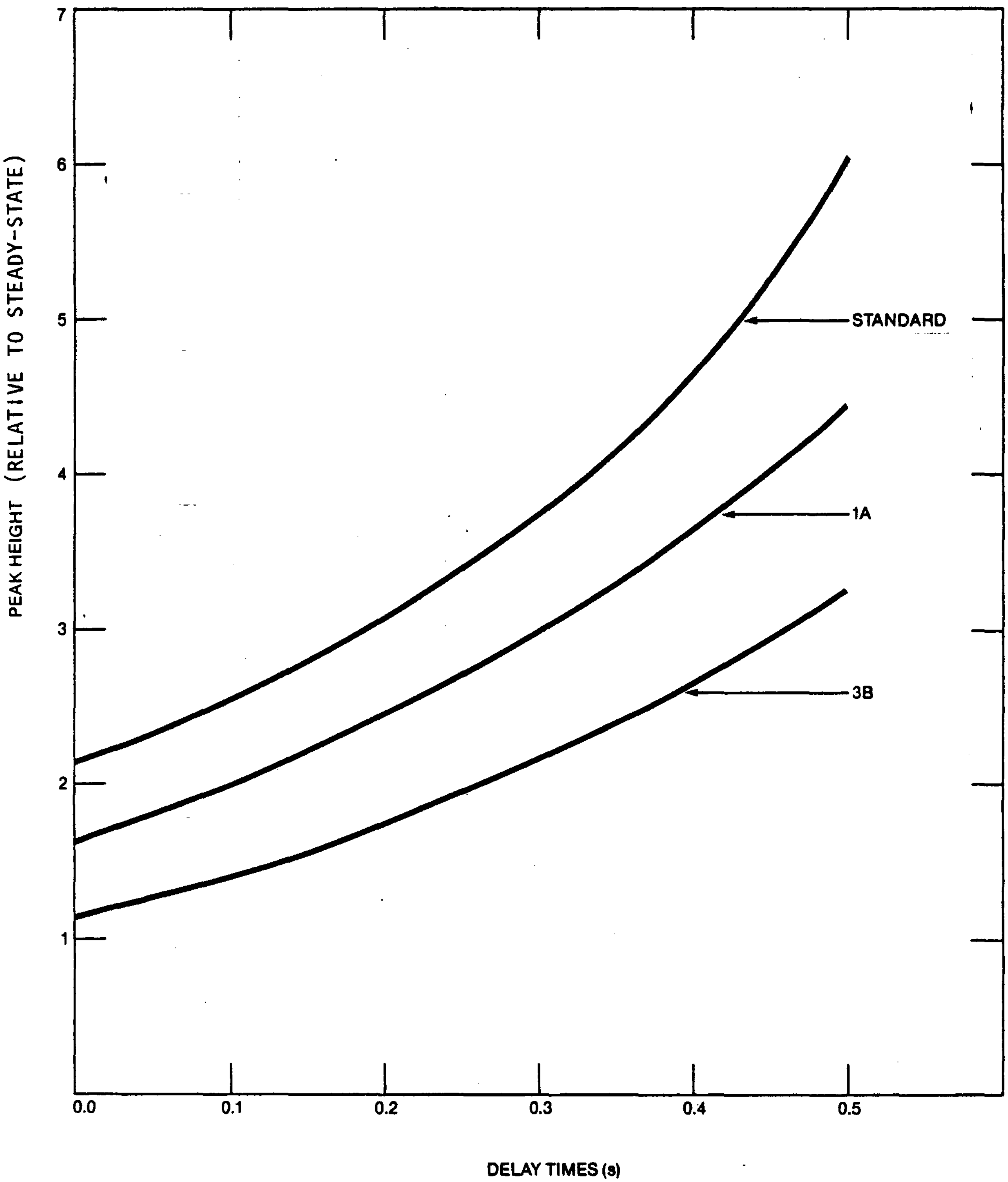

FIGURE 6.8 PEAK HEIGHT VERSUS DELAY TIMES

From the figures, the dependence of peak height and total energy production of the transients on the total delay time until initiation of shutoff rod movement is clearly illustrated. However, from a design basis, the effect of the rate of shutoff rod drop is a much more significant parameter. In terms of design and reactor safety, more can be gained by a more rapid insertion of the shutoff rods then by a reduction in delay time. This can be shown by comparing the standard case and Case 1A in Figure 6.4. From their drop curves, Case 1A is only a little faster than the standard rod as it is injected, and even lags behind the standard rod after 1.15 seconds. However, the action of it "biting" into the core earlier than the standard case has a significant effect on the subsequent transient. This effect is equivalent, at 0.4 seconds, to a 0.13 second reduction in delay time. To achieve this reduction in delay time would pose a much more difficult design problem than assisting the shutoff rod drop curve.

6.2 Effect of Delay-time on Poison Injection System

The power pulses following a LOCA for a 30% inlet header break were calculated for the second shutdown system. Two delay times, 0.35, seconds and 0.40 seconds, were initially studied. Figure 6.9 shows the two pulses obtained.

The similarity of the two pulses is evident. From Tables 6.1 and 6.2, the overall system reactivity, ρ_{total}, is:

$$\rho_{total} = \rho_{void} + \rho_{poison}$$

which after about 0.9 seconds is

$$\rho_{total} \sim \rho_{poison}$$

The large magnitude of the negative reactivity introduced by the injected poison overrides any contribution from the void reactivity, hence the major kinetic effects of the reactor core will closely follow the poison dynamic curve.

Thus, the separation of the two peaks (0.05 seconds) matches the differences in the delay times. The effect of the poison was considered so dominant that no further simulations were considered necessary in understanding this particular transient.

6.3 Effect of Fuel Burnup Distribution

Finally, the magnitude of the effect of space-dependent fuel burnup on the size of the power pulses was studied. This was done by carrying out two simulations for a 100% Pump Suction Break. In the first simulation, the reactor was modelled by having the channels that void rapidly after the break contain relatively fresh fuel. Due to the

TABLE 6.2 - SDS-2 PARAMETERS -0.40s DELAY

Time (s)	Dynamic Void Reactivity	SDS-2 Reactivity	Dynamic System Reactivity	Reactor Fission Power
0.07	0.0	0.0	0.0	1.000
0.12	0.451	0.0	0.451	1.011
0.22	1.509	0.0	1.509	1.098
0.35	3.020	0.0	3.020	1.339
0.40	3.605	0.0	3.605	1.477
0.50	4.270	0.0	4.270	1.818
0.60	4.700	0.0	4.700	2.228
0.70	4.720	0.0	4.720	2.669
0.80	4.850	-0.08	4.770	3.111
0.90	5.153	-0.100	5.053	3.614
1.03	5.522	-0.176	5.346	4.448
1.10	5.628	-2.286	3.342	4.600
1.16	5.698	-10.28	-4.582	3.442
1.22	5.773	-19.45	-13.67	1.615
1.28	5.851	-32.67	-26.81	0.533
1.34	5.937	-47.15	-41.21	0.217
1.39	6.012	-55.54	-49.52	0.155
1.45	6.107	-62.64	-56.53	0.128
1.50	6.139	-68.06	-61.92	0.114
1.55	6.139	-71.71	-65.57	0.104
1.60	6.120	-75.53	-69.41	0.097
1.65	6.082	-78.49	-72.40	0.090
1.70	6.042	-81.42	-75.37	0.085
1.75	5.998	-84.49	-78.49	0.080
1.81	5.945	-87.55	-81.60	0.075
1.86	5.898	-90.79	-84.89	0.071
1.99	5.778	-99.42	-93.64	0.062
2.05	5.772	-104.36	-98.58	0.058
2.50	5.316	-113.03	-107.71	0.046

TABLE 6.3 - SDS-2 PARAMETERS -0.35s DELAY

Time (s)	Dynamic Void Reactivity	SDS-2 Reactivity	Dynamic System Reactivity	Reactor Fission Power
0.07	0.0	0.0	0.0	1.000
0.12	0.451	0.0	0.45	1.011
0.22	1.509	0.0	1.509	1.098
0.35	3.020	0.0	3.020	1.339
0.40	3.605	0.0	3.605	1.477
0.50	4.270	0.0	4.270	1.818
0.60	4.700	-0.1	4.600	2.217
0.70	4.720	-0.1	4.620	2.632
0.80	4.850	-0.1	4.750	3.059
0.90	5.153	-0.1	5.053	3.561
1.03	5.522	-1.2	4.322	4.096
1.10	5.628	-9.0	-3.372	3.197
1.16	5.698	-18.0	-12.302	1.625
1.22	5.773	-34.5	-28.727	0.510
1.28	5.851	-46.5	-40.649	0.204
1.34	5.937	-55.5	-49.563	0.145
1.39	6.012	-62.0	-55.998	0.124
1.45	6.107	-68.0	-61.893	0.108
1.50	6.139	-71.7	-65.561	0.099
1.55	6.139	-75.5	-69.361	0.092
1.60	6.120	-78.5	-72.380	0.086
1.65	6.082	-81.4	-75.318	0.081
1.70	6.042	-84.4	-78.350	0.076
1.75	5.998	-87.4	-81.402	0.072
1.81	5.945	-90.7	-84.755	0.068
1.86	5.898	-93.7	-87.802	0.065
1.99	5.778	-103.5	-97.720	0.056
2.05	5.772	-107.0	-101.220	0.053
2.50	5.316	-113.0	-107.680	0.044

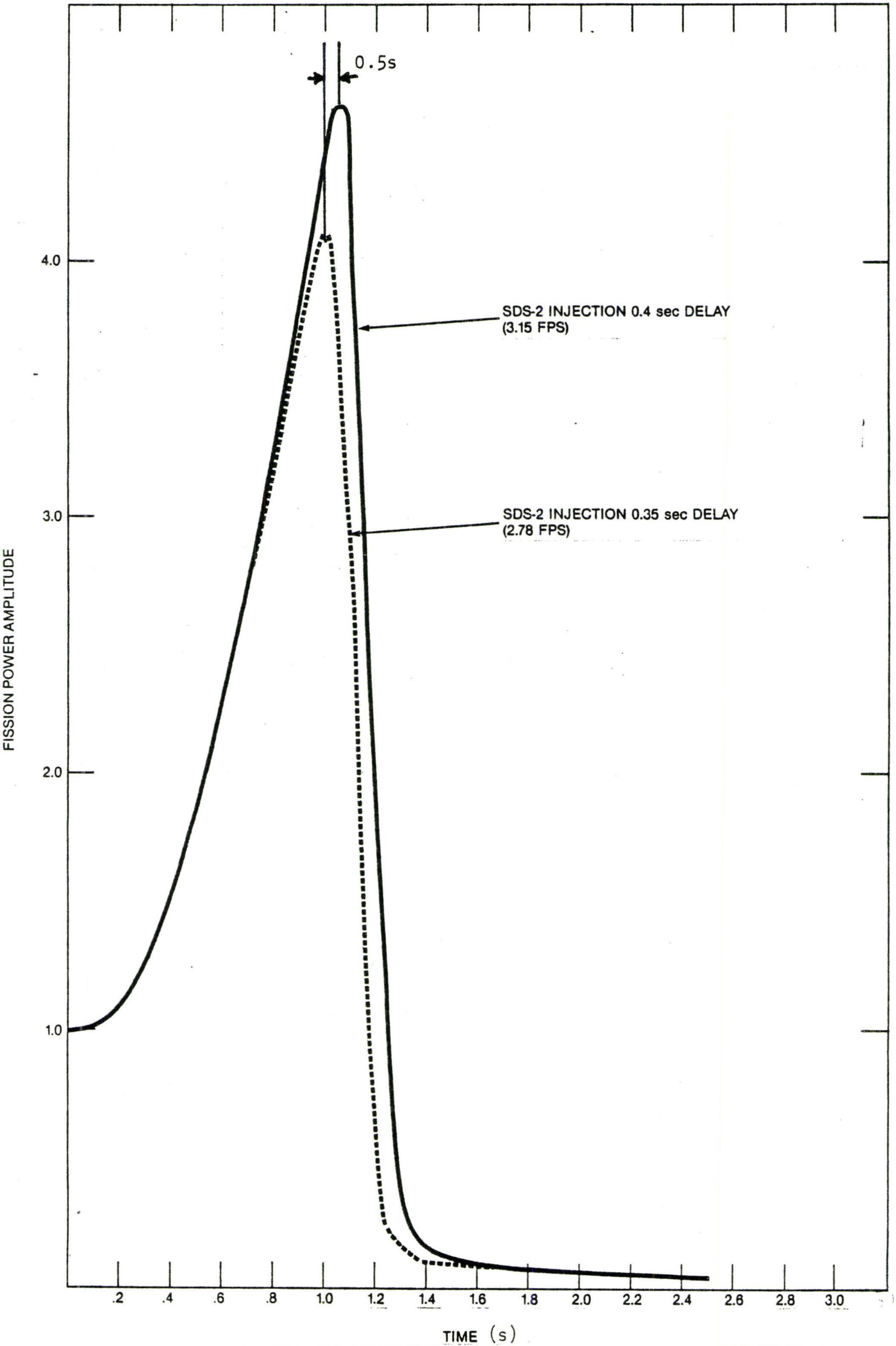

FIGURE 6.9 FISSION POWER AMPLITUDE vs TIME AFTER INLET HEADER BREAK

low concentration of plutonium isotopes in the voiding channels, this should give rise to a large void reactivity. However, the presence of a large delayed neutron fraction in fresh fuel will have an opposite effect on the power pulse. The second simulation assumed that the voiding channels contained relatively burned up fuel. In this case, the void reactivity should be small, but the small value of the delayed neutron fraction due to the higher concentration of plutonium isotopes should increase the system dynamic reactivity. The two simulations were run to determine the magnitude of the fuel burnup effect with respect to the power pulse.

A finite-difference code based on the improved quasistatic method was used in these simulations in order to model the spatial variation of the distribution of the void reactivity and delayed neutron fraction during the transient. A trip time of 0.32 seconds was used, and the dynamic reactivity used is shown in Figure 6.10. The simulation for the first case, i.e., voiding in the fresh fuel channels, was carried out until the shutoff rods were fully inserted into the core. The second case, voiding in the high burnup fuel channels, was run only until the power peak had been passed to save computation costs.

The results are shown in Figure 6.12. The power pulse for the fresh-fuel voiding is considerably higher than the high burnup case. Thus, the void reactivity due to the fuel irradiation or burnup is the dominant factor in determining the pulse size. The large difference in the two pulses resulted in a third simulation using an equilibrium fuel burnup distribution. This was to determine if the previous runs using such a distribution were closer to the fresh fuel or high burnup case.

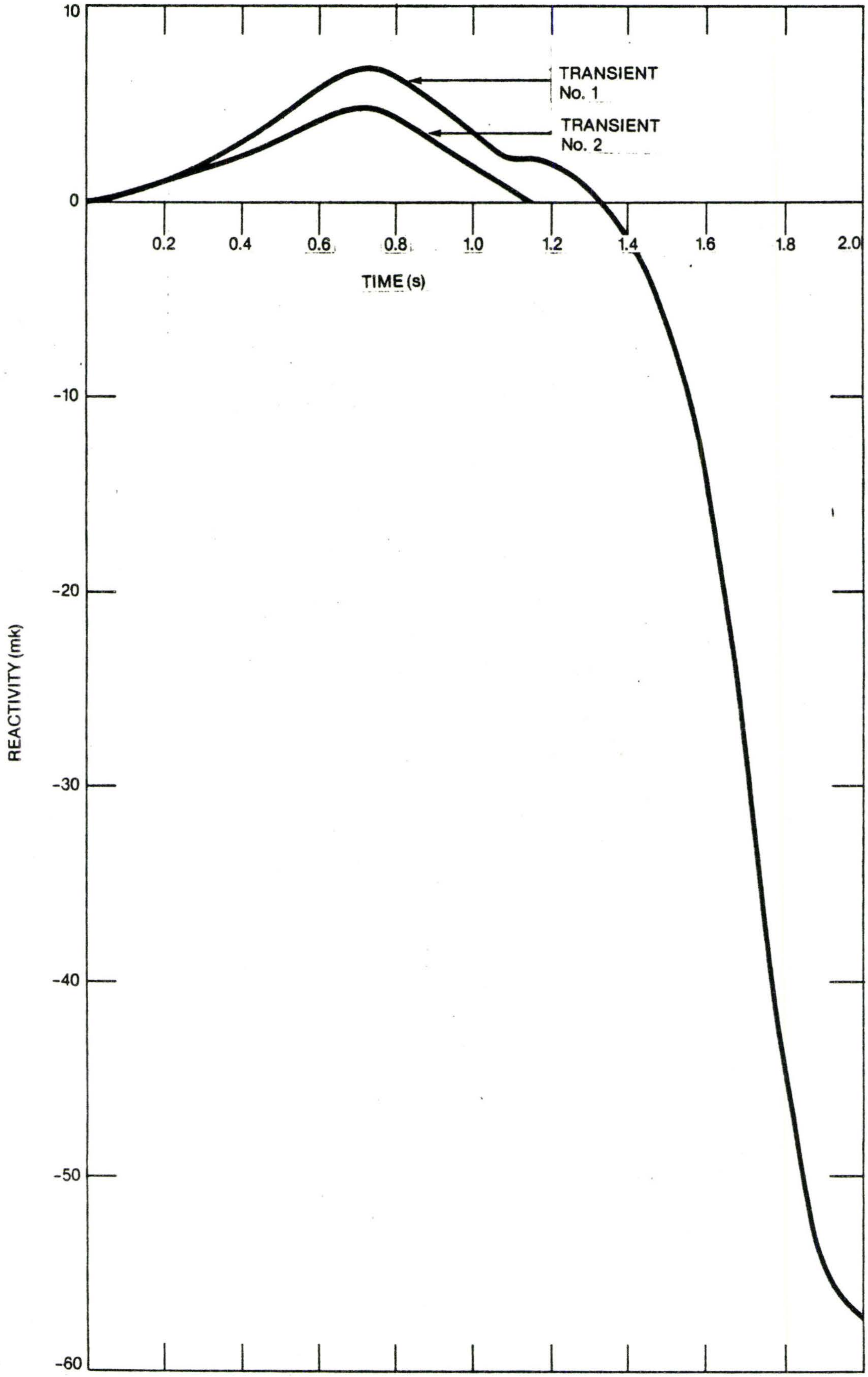

FIGURE 6.10 **DYNAMIC SYSTEM REACTIVITY**

TABLE 6.4: ABSOLUTE AND RELATIVE TOTAL POWER, TOTAL FULL POWER SECONDS, AVERAGE TOTAL BETA AND SYSTEM REACTIVITY (TRANSIENT 1)

Reactor Time (Seconds)	Total Power (Megawatts)	Relative Value	Total FPS	Effective Delayed Neutron Fraction	System Reactivity (milli-k)
0.0	2700.1	1.000	0.0		0.00
0.10	2709.0	1.003	0.1001	.598864E-2	0.725
0.32	3236.7	1.198	0.3369	.599528E-2	2.218
0.57	5435.8	2.013	0.7198	.602394E-2	5.443
0.65	6865.2	2.542	0.9011	.603291E-2	6.264
0.72	8548.9	3.166	1.1001	.604000E-2	6.819
0.79	10463.2	3.875	1.3466	.604319E-2	6.552
0.86	12156.7	4.502	1.6407	.604160E-2	5.877
0.92	13064.6	4.838	1.9222	.603704E-2	4.955
0.98	13263.2	4.912	2.2160	.603266E-2	4.053
1.03	12922.0	4.785	2.4591	.602979E-2	3.302
1.09	11888.5	4.403	2.7361	.602315E-2	2.046
1.14	10972.2	4.063	2.9473	.603039E-2	2.380
1.19	10223.3	3.786	3.1437	.602944E-2	1.941
1.24	9413.8	3.486	3.3257	.603081E-2	1.434
1.29	8542.6	3.163	3.4921	.603453E-2	0.788
1.34	7590.6	2.811	3.6417	.604004E-2	- 0.113
1.38	6716.3	2.487	3.7479	.604665E-2	- 1.460
1.43	5536.4	2.050	3.8614	.605510E-2	- 2.972
1.48	4397.8	1.628	3.9533	.606434E-2	- 4.992
1.52	3513.2	1.301	4.0119	.607329E-2	- 7.710
1.56	2673.5	0.990	4.0576	.608148E-2	-11.175
1.61	1826.6	0.676	4.0989	.608687E-2	-15.976
1.66	1237.5	0.458	4.1269	.608736E-2	-22.54
1.71	852.3	0.315	4.1460	.608356E-2	-30.90
1.77	597.3	0.221	4.1617	.607552E-2	-40.55
1.83	465.7	0.172	4.1734	.606563E-2	-49.20
1.89	395.3	0.146	4.1829	.605696E-2	-55.16
1.96	362.4	0.134	4.1926	.605351E-2	-56.76

TABLE 6.5: ABSOLUTE AND RELATIVE TOTAL POWER, TOTAL FULL POWER SECONDS, AVERAGE TOTAL BETA AND SYSTEM REACTIVITY (TRANSIENT 2)

Reactor Time (Seconds)	Total Power (Megawatts)	Relative Value	Total FPS	Effective Delayed Neutron Fraction	System Reactivity (milli-k)
0.0	2700	1.000	0.0		0.0
0.10	2707	1.002	0.100	.598810E-2	0.556
0.32	3113	1.153	0.333	.599148E-2	1.746
0.57	4439	1.644	0.675	.600648E-2	3.861
0.65	5128	1.899	0.816	.601065E-2	4.350
0.72	5823	2.156	0.958	.601405E-2	4.641
0.79	6451	2.389	1.118	.601457E-2	4.263
0.86	6801	2.519	1.290	.601183E-2	3.588
0.92	6777	2.509	1.442	.600700E-2	2.700
0.98	6440	2.385	1.589	.600254E-2	1.803
1.03	5983	2.215	1.704	.599962E-2	1.014
1.09	5375	1.990	1.831	.599798E-2	0.494
1.14	4882	1.808	1.926	.599731E-2	-0.102
1.19	4400	1.629	2.011	.599780E-2	-0.685

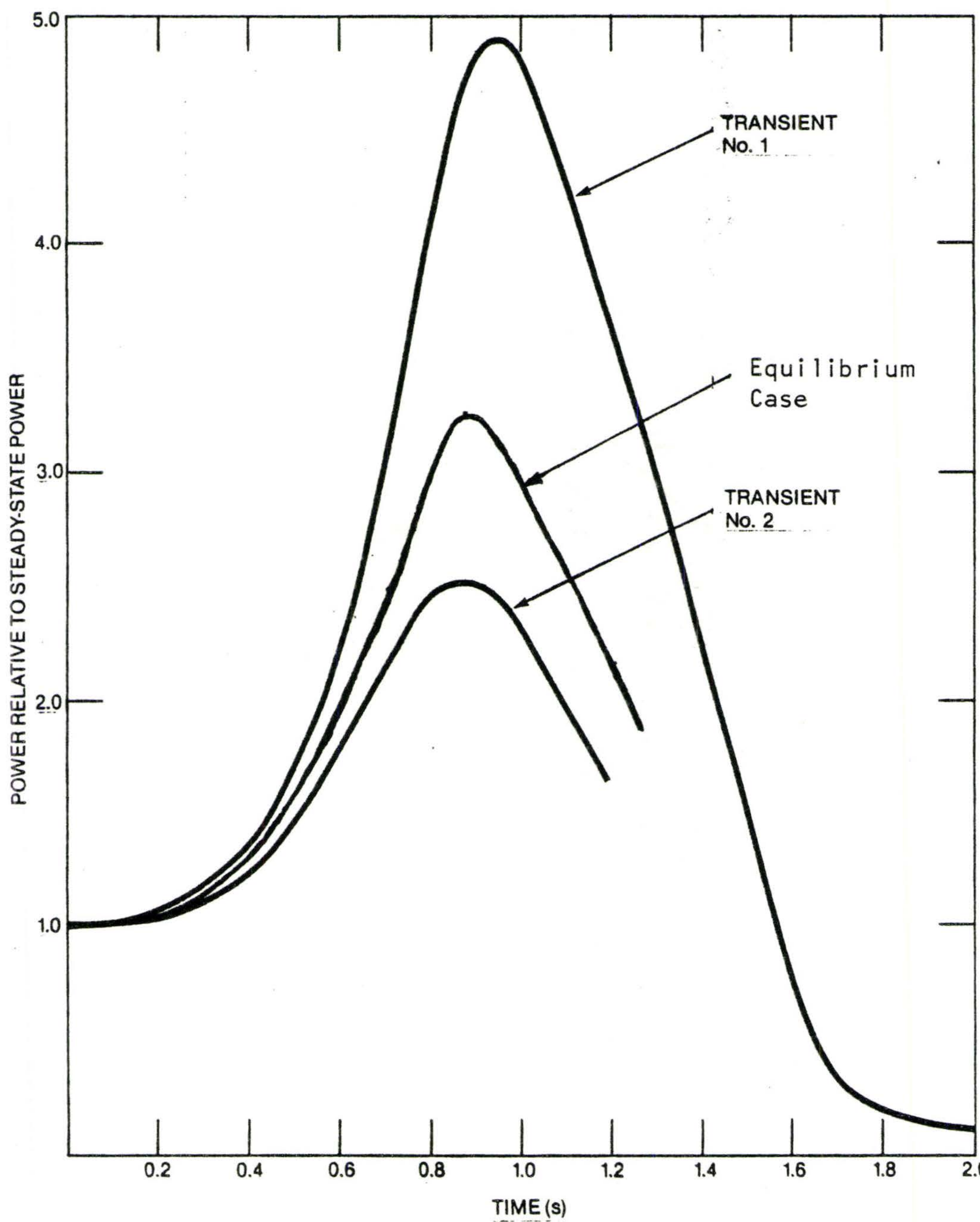

FIG. 6.11 **RELATIVE TOTAL POWER**

As shown in Figure 6.11, the equilibrium fuel case was closer to the high burnup case. This enabled a form of upper and lower bounds of the effect of fuel burnup to be determined for future simulations.

CHAPTER 7

CONCLUSIONS

The main conclusions of this study were:

i) Importance of delay times: As Figure 6.8 shows, increasing delay times result in an almost exponential increase in peak neutronic pulse height. This is especially significant for delay times greater than 0.3 seconds. Thus, from a design point of view, studies into reducing intrinsic detector system delays would be one means of further increasing the high safety factor of CANDU systems without the economic sacrifice which lower trip settings would induce (from more frequent spurious trips).

ii) Importance of fast initial entry of shutoff rods.
As seen from Figure 6.8 , the neutronic power peak heights were lower for all delay times for the shutoff rod drop curves which entered the core fastest. Especially significant is the comparison between the Standard (45.4 kg) Rod and the light assisted rod (18.1 kg) for Case 1A. Although the Standard case rod reached its final position faster than the lighter Case 1A rod, the effect of the lighter rod on the transients in their early stages more than compensated for both its smaller reactivity worth and slower drop rate near the reactor bottom. An analysis of assisted rod entry with even lighter rods but greater initial accelerations may indicate the optimal rod size-speed combination.

iii) Effect of delay time on SDS-2 system.

The large negative reactivity of the poison injection system dominated the neutron transients in Chapter 6.2. Hence, any reduction in delay time for the SDS-2 system is equivalent to a proportional decrease in peak height and peak height time of LOCA transients.

iv) Importance of fuel burnup distribution with respect to voiding channels.

Chapter 6.3 examined the magnitude of the fuel burnup distribution effect on neutronic power pulses. The significantly greater peak height for the fresh fuel voiding channel case (Transient 1 in Figure 6.11) as compared to both the equilibrium case and high burnup cases (Transient 2 in Figure 6.11) outlines the importance of proper parameter modeling of the burnup pattern of reactor cores, especially in the case of reactors during their first 100 full power days.

In summary, the influence of various neutronic parameters on the size and shape of power pulses resulting from loss of coolant accidents was examined in this report. It should again be noted that the type of accident postulated in this study, a Loss-of-Coolant accident, is an event of extremely low probability. Its use in reactor analysis ensures the design of reactor safety systems capable of responding to the fastest neutron transients possible.

REFERENCES AND BIBLIOGRAPHY

1. "CANDU Nuclear Power System", AECL Document TDSI-105, Sheridan Park, January (1981).

2. Dastur, A.R. and Buss, D.B., "Space-Time Kinetics of CANDU Systems"; Proceedings of Specialists' Meeting on New Developments in Three-Dimensional Neutron Kinetics and Review of Kinetics Benchmark Calculations, Garching, West Germany, 22-24 January (1975).

3. Glasstone, S. and Sesonske, A., "Nuclear Reactor Engineering"; Van Nostrand Reinhold Company, New York (1967).

4. Henry, A.F., "Nuclear Reactor Analysis"; MIT Press, Cambridge, Mass. (1975).

5. Lamarsh, J.R., "Nuclear Reactor Theory"; Addison-Wesley, Reading, Mass. (1972).

6. Pasanen, A.A., "Fundamental of CANDU Reactor Nuclear Design - A Lecture Series given at Trieste 22 January - 28 March 1980", AECL Document TDAI-244, Sheridan Park, August (1980).